The Astrophysical Journal Supplement Series, 244:15 (23pp), 2019 September https://doi.org/10.3847/1538-4365/ab3662

Bright Southern Variable Stars in the bRing Survey

Samuel N. Mellon[1], Eric E. Mamajek[1,2], Remko Stuik[3], Konstanze Zwintz[4], Matthew A. Kenworthy[3], Geert Jan J. Talens[5], Olivier Burggraaff[3,6], John I. Bailey, III[7], Patrick Dorval[3], Blaine B. D. Lomberg[8,9], Rudi B. Kuhn[8], and Michael J. Ireland[10]

[1] Department of Physics & Astronomy, University of Rochester, 500 Wilson Blvd., Rochester, NY 14627, USA; smellon@ur.rochester.edu
[2] Jet Propulsion Laboratory, California Institute of Technology, M/S 321-100, 4800 Oak Grove Dr, Pasadena, CA 91109, USA
[3] Leiden Observatory, Leiden University, P.O. Box 9513, 2300 RA Leiden, The Netherlands
[4] Institut für Astro- und Teilchenphysik, Universität Innsbruck, Technikerstrasse 25/8, A-6020 Innsbruck, Austria
[5] Institut de Recherche sur les Exoplanètes, Département de Physique, Université de Montréal, Montréal, QC H3C 3J7, Canada
[6] Institute of Environmental Sciences (CML), Leiden University, P.O. Box 9518, 2300 RA Leiden, The Netherlands
[7] Department of Physics, University of California at Santa Barbara, Santa Barbara, CA 93106, USA
[8] South African Astronomical Observatory, Observatory Rd, Observatory Cape Town, 7700 Cape Town, South Africa
[9] Department of Astronomy, University of Cape Town, Rondebosch, 7700 Cape Town, South Africa
[10] Research School of Astronomy and Astrophysics, Australian National University, Canberra, ACT 2611, Australia
Received 2019 July 15; revised 2019 July 25; accepted 2019 July 27; published 2019 September 11

Abstract

In addition to monitoring the bright star β Pic during the near-transit event for its giant exoplanet, the β Pictoris b Ring (bRing) observatories at Siding Springs Observatory, Australia and Sutherland, South Africa have monitored the brightnesses of bright stars ($V \simeq 4$–8 mag) centered on the south celestial pole ($\delta \leqslant -30°$) for approximately two years. Here we present a comprehensive study of the bRing time-series photometry for bright southern stars monitored between 2017 June and 2019 January. Of the 16,762 stars monitored by bRing, 353 were found to be variable. Of the variable stars, 80% had previously known variability and 20% were new variables. Each of the new variables was classified, including three new eclipsing binaries (HD 77669, HD 142049, HD 155781), 26 δ Scutis, 4 slowly pulsating B stars, and others. This survey also reclassified four stars based on their period of pulsation, light curve, spectral classification, and color–magnitude information. The survey data were searched for new examples of transiting circumsecondary disk systems, but no candidates were found.

Unified Astronomy Thesaurus concepts: Variable stars (1761); Multi-periodic variable stars (1079); Long period variable stars (935); Short period variable stars (1453); Eclipsing binary stars (444); Ellipsoidal variable stars (455)

1. Introduction

Over the past two decades, several wide-field, ground- and space-based surveys have contributed countless hours of observations in the night sky (e.g., KELT, MASCARA, NASA's *Kepler* and *K2* space missions: Pepper et al. 2007; Borucki et al. 2010; Howell et al. 2014; Talens et al. 2017b). The primary goal of these surveys has been the discovery of exoplanets, with each having a number of significant successes (e.g., Oberst et al. 2017; Talens et al. 2017a). A secondary result from these surveys has been the discovery and characterization of variable stars (e.g., Burggraaff et al. 2018; Collins et al. 2018).

Variable stars form the cornerstone of much of the knowledge about our universe, such as asteroseismology (e.g., Zwintz et al. 2014a, 2014b), stellar gyrochronology and rotation (e.g., Hartman et al. 2010; Gallet & Bouvier 2013; Cargile et al. 2014; Mellon et al. 2017), classical Cepheids as standard candles for distance (e.g., Groenewegen 2018), and eclipsing systems (e.g., Mellon et al. 2017; Collins et al. 2018; Moe & Kratter 2018). In addition to the exoplanet surveys, dedicated variable star observatories and online catalogs have fueled research in these areas (e.g., ASAS, AAVSO, ASAS-SN, OGLE: Pojmanski 2002; Watson et al. 2006; Udalski et al. 2008; Shappee et al. 2014). Physical properties of stellar systems can be constrained from the period and amplitude of the observed variability, such as the composite sinusoidal variability observed in the δ Scuti star β Pictoris (Mékarnia et al. 2017; Zwintz et al. 2019).

In 2017, the β Pictoris b Ring (bRing) instruments (located in South Africa and Australia) were constructed and brought online to observe the 2017–2018 transit of the β Pictoris b Hill sphere (Stuik et al. 2017; Kalas et al. 2019; Mellon et al. 2019b). While observing β Pictoris, bRing captured nearly continuous photometry of 10,000+ bright stars ($V \sim 4$–8 mag) in the southern sky ($\delta \leqslant -30°$). In addition to the study of the β Pictoris b Hill sphere, the bRing survey has contributed to the discovery of δ Scuti pulsations in the A1V star HD 156623 (Mellon et al. 2019a), the study of β Pictoris' δ Scuti pulsations (Zwintz et al. 2019), and the discovery of the retrograde hot Jupiter MASCARA-4 b/bRing-1 b (Dorval et al. 2019).

In this work, we took a similar approach to the MASCARA survey of the northern sky (Burggraaff et al. 2018) and searched for periodic variations in the bRing data. This survey was also sensitive to evidence of transiting circumplanetary systems like "J1407" (V1400 Cen; Mamajek et al. 2012), or other circumsecondary disks; however, none were found. Section 2 of this work describes the data from both the South African bRing (bRing-SA) and Australian bRing (bRing-AU) stations. Section 3 details the analysis used to identify and characterize both the regular and irregular variables in the data. Section 4 provides tables and discussions of each type of variable found in cross-correlation with the VSX catalog (Watson et al. 2006) and others.

2. Data

The data in this work were collected between 2017 June and 2019 January by the bRing-SA and bRing-AU stations. Each

station had two stationary cameras; one camera faced southeast (Az = 150°; SAE and AUE) and the other southwest (Az = 230°; SAW and AUW). Each camera had an FLI 4008 × 2672 pixel CCD and $f = 1.4$ mm Canon wide-angle lens, which resulted in a total field of view of 74° × 53° with a pointing optimized for β Pictoris ($\delta \simeq -53°$). Exposure times were alternated between 6.4 and 2.54 s; these were subsequently coadded and binned to 5 minute samplings and saved to disk (Stuik et al. 2017; Talens et al. 2018).

Due to bRing's large pixel size (~1 arcmin^2), blending was a significant issue for bRing. Blending was evaluated by comparing the relative brightnesses of stars located within the same bRing inner aperture (radius = 2.′5) as the target star (nearby stars evaluated with the ASCC catalog; Kharchenko 2001). For stars with previously known variability, blending was ignored if the original period was detected, but considered if a second period was detected or dominated the expected period. If a second period dominated the expected period in a blended star, the star was reanalyzed at the original expected period. If a star showed signs of variability in our light curves and had been previously unidentified as a variable in other surveys, blending was required to be 0 to be considered a detection. Ultimately, 16,762 stars were analyzed for this work. The stars listed in this work as new variables had no evidence of blending in their light curves.

On average, a star had observations spanning over 300 days (each star ideally received 21 hr of continuous coverage per day); the average star had ~20,000 five minute binned data points over the entire observing window combined from all four cameras. More information on the bRing observing strategy and data calibration can be found in Stuik et al. (2017) and Talens et al. (2018). In conjunction with this work, the camera .FITS files for each star (as described in Stuik et al. 2017) were published in a Zenodo repository at doi:10.5281/zenodo.3341783.

In interpreting the nature of the variability, *BV* photometry was drawn from the ASCC-2.5 catalog (Kharchenko 2001) and spectral types were drawn from the literature, with most types taken from the Michigan Spectral Survey of classifications from objective-prism plates (Houk & Cowley 1975; Houk 1978, 1982). Houk et al. (1997) has shown that for $V < 8$ mag stars classified as dwarf luminosity class in the Michigan Spectral Survey, for a given 2D spectral type the intrinsic color spread rms in $B - V$ is ~0.03–0.04 mag and the intrinsic spread in absolute V magnitudes is ~0.4–0.5 mag, with distributions suggesting negligible contamination by more evolved giants and supergiants. The Michigan classifications for the variable stars have quality flags of 1 (61.6%), 2 (28.9%), 3 (7.0%), and 4 (0.6%), with the 93% flagged as quality 1 and 2 considered the "higher-quality" classifications (Houk 1978; Houk et al. 1997).

3. Analysis

The 5 minute binned data points from bRing were automatically calibrated and detrended for temporal and spatial effects from the observations (e.g., clouds, intra-pixel variations; Stuik et al. 2017; Talens et al. 2018). Using an internal custom pipeline detailed in Mellon et al. (2019a), these data were downloaded from the bRing server and further detrended for sidereal and lunar systematics as well as astrometric and color systematics. This routine also includes a barycentric correction. In addition to the detrending from previous works, we attempted to preserve the ansatz period prior to detrending by including an additional step adopted from Burggraaff et al. (2018). The data for each star from each of the four bRing cameras were treated individually and then median-combined after detrending.

3.1. Identifying the Ansatz Period

The time-series photometry data were analyzed using the reduction pipeline previously used and described in Mellon et al. (2019a), with a modification based on the study by Burggraaff et al. (2018). The step adopted from Burggraaff et al. (2018) to improve upon the process from Mellon et al. (2019a) was the initial identification and removal of an ansatz period from the data prior to detrending. The goal of this step was to preserve any real and significant periods from being affected by the detrending process. To find the ansatz period, a normalized Lomb–Scargle periodogram (Scargle 1982; Press et al. 1992) was generated using the ASTROPY (The Astropy Collaboration et al. 2018) library. Next, a Python routine was written using tools available in the SCIPY (Jones et al. 2001), NUMPY (Stéfan van der Walt & Varoquaux 2011), and ASTROPY packages to identify the strongest periods in the periodogram. These periods were then compared to the well-studied sidereal and lunar systematics present in the bRing data (the origins of these systematics and methods for removing them are thoroughly discussed in Stuik et al. 2017; Burggraaff et al. 2018; Talens et al. 2018; Mellon et al. 2019a). The strongest period that was not within 5% of one of these systematics (or the corresponding harmonics and aliases to order 5) was accepted as the ansatz period, fit with a sine, and removed from the light curve. This information was stored and was added back in after detrending.

3.2. Detrending and Measurement of Variable Star Parameters

The detrending routine used after the removal of ansatz period is described in Mellon et al. (2019a) and is summarized in this work. First, an astrometric correction was applied to remove data points that deviated $>3\sigma$ from the mean path of the star on the CCD. Then, the time series was adjusted to the barycentric reference frame and a second-order CCD color correction was applied to the data. The best ansatz signal was then determined and temporarily removed from the data. Next, a median-binning routine was used to significantly reduce the strength of the lunar and sidereal systematic signals. After detrending, the ansatz signal was added back into the light curve and a composite light curve was generated from the four camera light curves using a median alignment. A new periodogram was calculated from this composite light curve. Finally, a plot of the composite light curve, a periodogram, and a phase-folded light curve on the most likely variability period was generated for analysis. These plots were used to identify variables in the data by eye. An example is plotted in Figure 1 for the δ Scuti HD 156623. The plots generated for this work were included in the same Zenodo repository, doi: 10.5281/zenodo.3341783, as the data.

The measurements and information used to construct the tables of variable stars (see Section 4) were also generated. The best periods for variables were taken directly from the composite light-curve periodograms and verified by comparing measurements from the four independent camera data sets. A previously unseen frequency was accepted if it was detected in

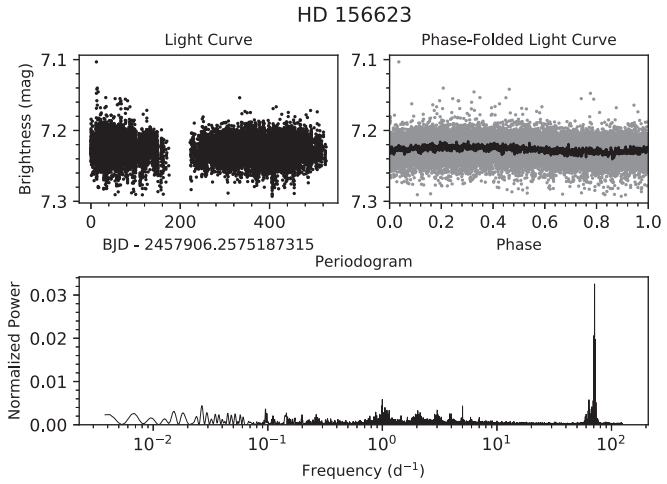

Figure 1. Example plot of the δ Scuti HD 156623. The top left panel contains the light curve of the star. The top right panel contains the light curve of the star (gray dots) phase-folded on the primary period with a running median fit (solid curve). The bottom panel contains the normalized LS periodogram.

at least one camera from each site. Uncertainties for the frequencies were measured from the standard deviation in the detected frequencies; amplitude uncertainties were calculated using methods from Montgomery & Odonoghue (1999). We compared the Montgomery & Odonoghue (1999) frequency uncertainty measurements to the measurements from using the four camera data sets and found the uncertainties were typically underestimated by a factor of ∼5. This is expected, as the uncertainties from Montgomery & Odonoghue (1999) were noted in their work as lower limits on the errors in these measurements.

3.3. False Positives

The strongest periodogram frequencies from the stars in this study were used to identify remaining low-frequency ($f < 1.5\,\mathrm{day}^{-1}$) and high-frequency ($f > 1.5\,\mathrm{day}^{-1}$) false positives due to systematics in the bRing system. To do this, a density plot of the strongest frequencies was generated with bin sizes of $0.01\,\mathrm{day}^{-1}$ (Figure 2). The left panel focuses on the low-frequency false positives, which have been discussed thoroughly in Stuik et al. (2017), Talens et al. (2018), Burggraaff et al. (2018), Mellon et al. (2019a). The high-frequency systematics were observed to be more numerous and scattered, but are weaker by a factor of ∼10 compared to the low-frequency systematics and are roughly a factor of 10 above the noise floor ($\simeq 10^{-4}$) of the plot. Possible sources include the $288\,\mathrm{day}^{-1}$ (5 minute) sampling frequency of bRing and its beats/aliases and electromagnetic interference within bRing. The bRing detrending routines are continuing to be internally developed to minimize the effects of these dominating systematics.

The low-frequency systematics posed the largest problem due to the majority of the variables in this survey having real frequencies in this regime. They are clearly dominated by the sidereal cycle and its aliases; the large peaks that pick up around 0.167 day are due to the ansatz routine not picking up frequencies at that harmonic. We were careful when reporting frequencies as real when they were within $0.1\,\mathrm{day}^{-1}$ of these frequencies. For example, if independent evidence of variability existed for these frequencies near a systematic (e.g., the eclipsing binary (EB) V397 Pup with a 3.00402 day period; Watson et al. 2006), they were accepted as real. However, potential new variables could have been missed due to the lack of a sophisticated means of independent verification or imperfections in the detrending or ansatz routines. The high-frequency systematics were only applicable to the δ Scuti candidates due to their high-frequency regime; however, the systematics were not an issue for the δ Scuti primary frequencies detected in this study.

3.4. Performance Analysis

The sample from this study was also used to study the performance of bRing. In Figure 3, the rms for each post-detrending star was plotted in gray against the catalog magnitude of the star. For each camera, ∼14% of the stars performed better than 1% and ∼70% stars performed better than 2% (dashed line). The results here are similar to the results from Talens et al. (2017b, 2018).

By visual inspection, it is clear that a combined noise floor (plotted as a horizontal dotted–dashed line in Figure 3) exists in all 4 cameras at an rms of about 0.005. The region brighter than $V \simeq 5.5$ mag is dominated by this combined noise floor term. Contributing terms to this noise floor include scintillation noise (estimated to be around 10^{-4} at both sites via Young's approximation: Young 1967; Osborn et al. 2015), noise contributed from the calibration and detrending, as well as other noise sources such as read noise and dark current. This noise floor level matches the expected photometric precision for bright stars in bRing, indicating that the detrending routine used in this work was successful (Stuik et al. 2017; Talens et al. 2017b, 2018). The fainter region was dominated by the shot noise and sky noise contributions. Overall, bRing performed as expected at the bright end and performed well for stars at the faint end, which made a complete survey of all the stars in the bRing data possible despite lingering systematics.

4. Results and Discussion

We detected 353 variable stars in the bRing survey. We used the VSX[11] catalog, Vizier,[12] and SIMBAD[13] web services to identify previously known or candidate variables (Ochsenbein et al. 2000; Wenger et al. 2000; Watson et al. 2006). The periods reported for previously known variables were then compared to the periods detected with bRing. Stars that had no mention as variable stars in these databases, or suspected variables that did not have quoted periods in any source, are reported here as new periodic variables. Of the 284 previously known variables in this survey, the bRing periods were found to be consistent for 62% of the stars. The majority of the inconsistent periods were δ Scutis or long-period variables (LPVs). bRing could simply be detecting a more significant period or alias for the δ Scutis due to their multi-periodic nature that requires further study to disentangle (out of the scope of this work). The LPVs typically had low-precision measurements of the period, leading to the inconsistencies observed between previous measurements and bRing measurements.

bRing detected 71 variables that had not been previously flagged as known or candidate variables (including the 17 irregular variables observed by bRing). bRing was also able to reclassify four stars based on their newly measured period, light-curve shape,

[11] The VSX catalog is regularly updated at https://www.aavso.org/vsx/.
[12] https://vizier.u-strasbg.fr/
[13] http://simbad.u-strasbg.fr/simbad/

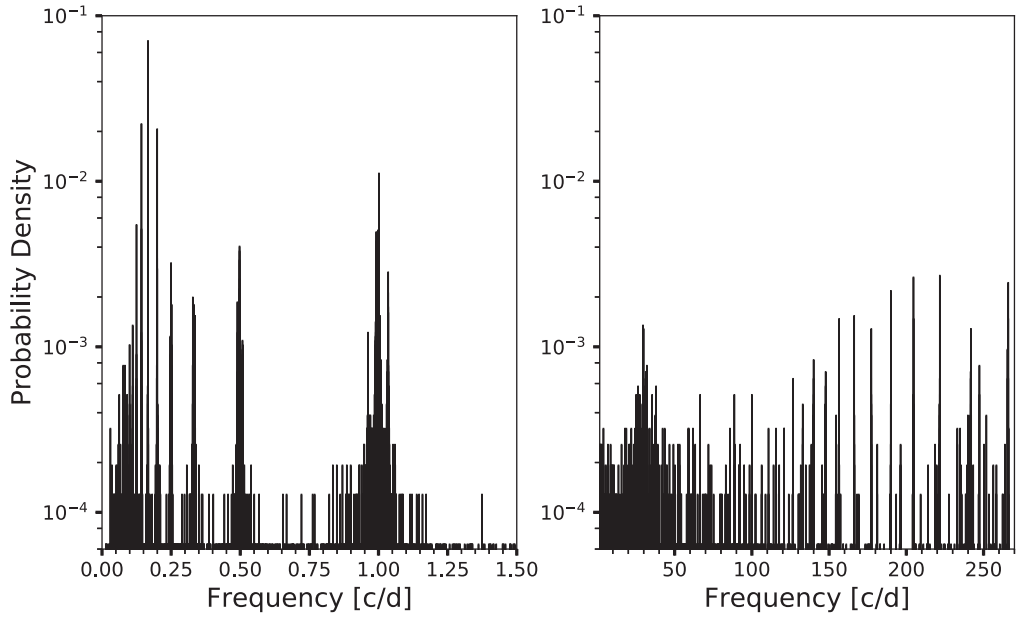

Figure 2. Probability density plot of the strongest frequencies in the periodograms of all the stars in this study. The left panel focuses on low-frequency (0–1.5 day^{-1}) pulsations with clear contributions at 1 day^{-1} and its aliases. The right panel contains higher frequencies (>1.5 day^{-1}) and has notable contributions at ∼30 day^{-1}, 100 day^{-1}, 200 day^{-1} and their beats and aliases. The noise floor of the plot is at a probability density of ∼10^{-4}. It is worth noting the low-frequency systematics are at least an order of magnitude stronger than the high-frequency systematics, which are themselves an order of magnitude stronger than the noise floor.

and spectral classification. The remainder of the stars showed no detectable or independent signs of variability down to the ∼1 mmag level. These stars are tabulated by variable classification in the following subsections.

The color-absolute magnitude positions of the 353 variable stars are plotted in Figure 4. The different types of variables are symbol-coded with respect to the tables they inhabit in Section 4. Previously known variables are outlined in black, while newly identified variables are solid black. For the four stars that are reclassified in this work, a small black star was placed on top of their respective symbols. The SIMBAD service was queried for Johnson *BV* photometry (Perryman & ESA 1997; Kharchenko 2001), Galactic coordinates l and b, and in the vast majority of cases, either a *Gaia* DR2 or *Hipparcos* parallaxes (Ochsenbein et al. 2000; van Leeuwen 2007; Brown et al. 2018). We queried the most recent 3D reddening maps from the STILISM[14] program to deredden the $(B-V)$ colors (Capitanio et al. 2017; Lallement et al. 2018). Following Mellon et al. (2019a), we adopted the ratio of total to selective extinction to be $A_V/E(B-V) \simeq 3.07 + 0.167\,(B-V)_o$, which is an adequate approximation over the intrinsic color interval $-0.32 < (B-V)_o < 1.5$. Solar composition PARSEC isochrones (Bressan et al. 2012; Marigo et al. 2017) were overlaid for several ages; these were generated using the CMD 3.3 Input tool.[15] The color-absolute magnitude parameters calculated for Figure 4 are tabulated in Table 10 in the Appendix.

4.1. Cepheid Variables

A total of 47 previously classified Cepheid variables detected with bRing have well-defined periods in the VSX catalog. These are tabulated in Table 1, which includes identification information about each star, the primary bRing period and amplitude, and the reported VSX period. This structure is used for tables throughout this paper. The primary frequencies recovered by bRing agreed with all of the fundamental modes reported in the VSX catalog. A future study of Cepheids in bRing could yield fainter frequency modes present in their power spectrum and help identify the Blažhko effect if present (Blažko 1907). Based on their CMD position (Figure 4), two of the stars are unusual for Cepheids; we reclassify them.

HD 132247 (ASAS J145955-4957.9) is a A0IV star (Houk 1978) classified in VSX as both a first-overtone classical Cepheid and an α^2 Canum Venaticorum (ACV) (Sitek & Pojmański 2014). This is a poorly studied star that does show an 8 mmag pulsation at a period of 2.123 days. There are other modes present in the star's periodogram; however, nothing is indicative of it being a classical Cepheid in addition to its spectral classification. Although its period could indicate this is an ACV variable, a lack of spectral observations to identify chemical peculiarities and spectral line intensity variations make it challenging to unambiguously classify.

One possible variable classification is a δ Scuti. Although the luminosity class of the star suggests it lies beyond the blue edge of the instability strip (Breger & Pamyatnykh 1998), its position in Figure 4 ($(B-V)_0 = 0.13$, $M_V = 1.40$) is on top of the other δ Scutis in this study. In addition, δ Scutis have been shown to exist blueward of this theoretical limit (Bowman & Kurtz 2018; Mellon et al. 2019a). Therefore, the classical Cepheid designation should be removed. The ACV designation should also be changed due to lack of a detailed spectral study. It is reasonable to suggest that this star is actually a δ Scuti based on its CMD position and multiple pulsation modes present in its periodogram.

HD 136633 (ASAS J152459-6156.7) is a B3V star (Houk & Cowley 1975) classified as a fundamental-mode classical Cepheid in VSX (from Sitek & Pojmański 2014). The periodogram does reveal multiple modes present; however, the B3V spectral classification means this star astrophysically is unlikely to be a classical Cepheid. It is more likely to be a β

[14] https://stilism.obspm.fr/
[15] http://stev.oapd.inaf.it/cgi-bin/cmd

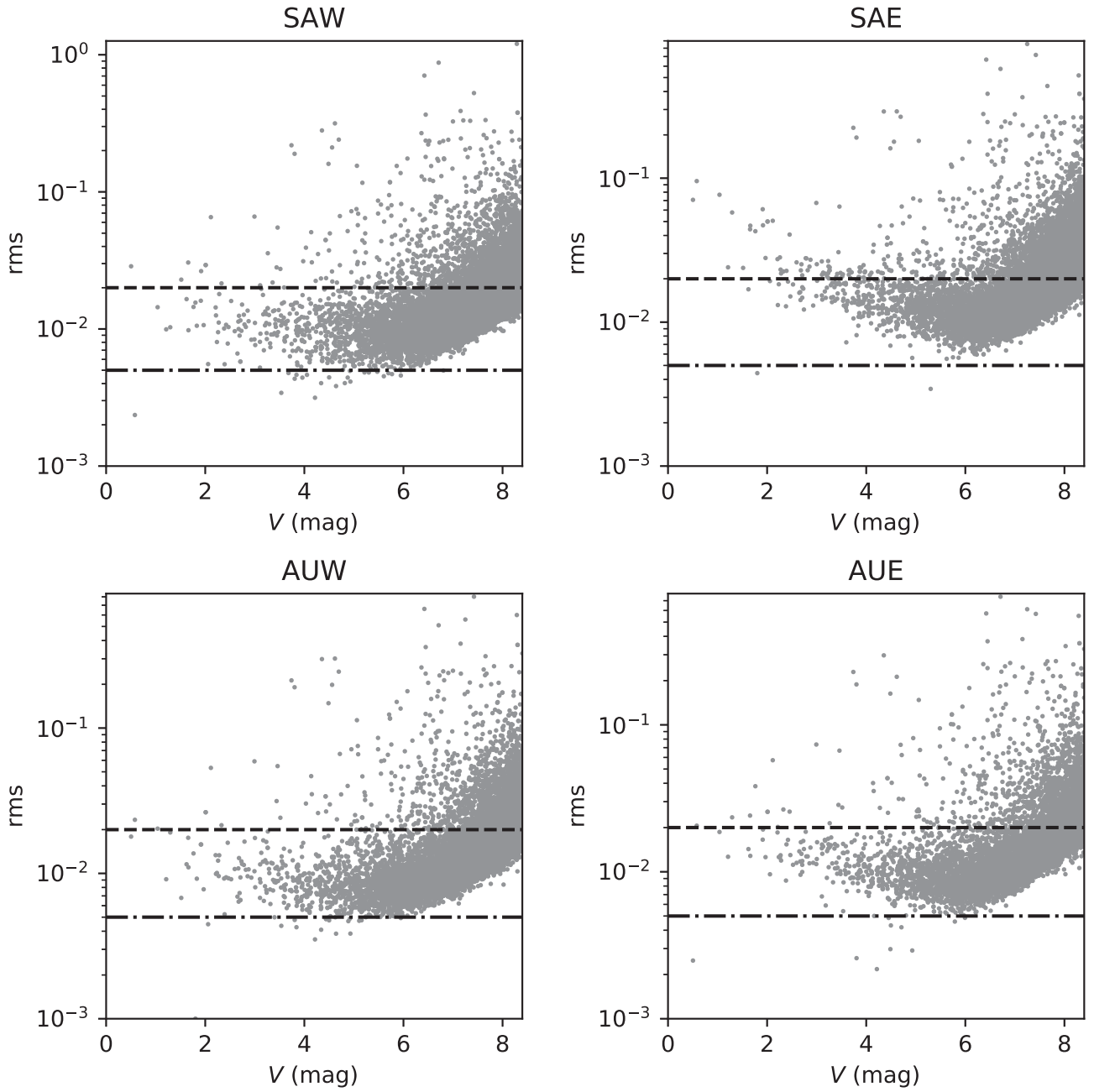

Figure 3. Plots showing the rms (gray dots) in each of the cameras for the 16,762 stars in this survey. The horizontal dashed line represents 2% scatter. The horizontal dotted–dashed line represents the combined noise floor estimated by visual inspection to be at an rms of around 0.005.

Cephei (BCEP) or slowly pulsating B-type (SPB) star. This agrees with its position on the CMD (Figure 4: $(B-V)_0 = -0.12$, $M_V = -2.00$). The modes present in this star appear to better fit the description of an SPB and should be reclassified as such (De Cat 2007; Miglio et al. 2007).

4.2. EBs and the O'Connell Effect

We detected 120 EBs in the bRing data set. For most of these EBs, the periodogram revealed the half period (the phase-folded light curve showed the primary and secondary eclipses overlapping) as the dominating sinusoidal component. When a potential EB was found, the periodogram was rescanned in a window around double the original period to find the true period. For a few EBs, this was not true and the correct period was searched for manually. The known EBs were discussed in Section 4.2.1 and are tabulated in Table 2 like the Cepheids in Table 1. Periods from Rimoldini et al. (2012) were used in place of missing VSX periods where available. Three new EBs are discussed in Section 4.2.2 and summarized in Table 3. Eighteen of the bRing EB light curves also showed evidence of the O'Connell effect (O'Connell 1951), and these are discussed in Section 4.2.3 and their parameters are summarized in Table 4.

4.2.1. Previously Identified EBs

For the 117 variable stars previously classified as EBs, the measured periods were compared to the values listed in the VSX catalog. The periods we measured with bRing agreed with

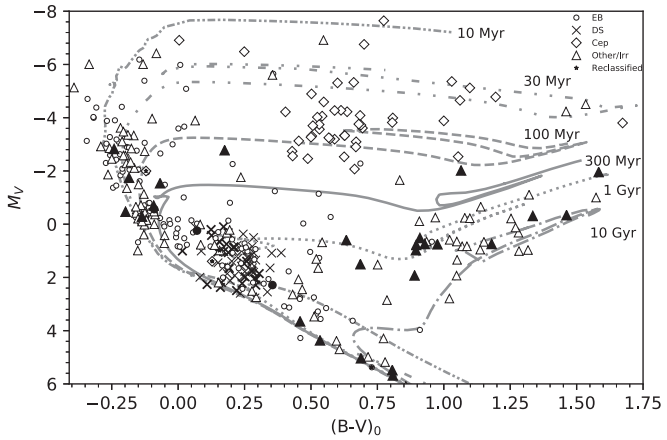

Figure 4. Color–magnitude diagram of the variables in this work. Types of variables are symbol-coded with respect to the tables presented in Section 4. The symbols for previously identified variables are outlined in black and newly identified variables are solid black. The four reclassified variables in this work are denoted with a black star. Several solar composition PARSEC isochrones are overlaid (Bressan et al. 2012; Marigo et al. 2017). Two of the stars had reddening values that placed them outside the scope of this plot; these stars were not plotted in order to better focus on the majority of the stars HD 85871 ($(B-V)_0 = 2.32$, $M_V = -3.45$) and HD 30551 ($(B-V)_0 = 2.63$, $M_V = -3.99$). Another star (HD 69342) was not included because a distance could not be determined for this star.

95 (∼81%) of the periods reported in VSX within 1%. There were 9 stars (∼7%) whose bRing periods were double the VSX period, but for which we confirmed the bRing periods by visual inspection of the phase-folded light curve (DV Gru, BR Ind, V452 Car, HD 66623, HD 205877, HD 56910, V376 Pup, HR Lup, R Ara). For eight stars (∼7%) a different period was detected that reproduces the eclipse structure, whereas the VSX period does not (V361 Pup, HD 70999, V360 Pup, V2509 Sgr, V661 Car, HD 16589, NO Pup, HD 203244). There were also five stars (∼5%) whose bRing periods recovered the eclipsing structure at half the reported VSX period (DE Mic, HD 129094, X Car, V535 Ara, V831 Cen). We further discuss a couple of notable cases: HD 70999 and HD 203244.

HD 70999: unfortunately, the VSX period for this star was near one of the strong, low-frequency bRing systematic false positives (see Section 3.3). The light curve also seemed to be missing the eclipses for ∼25% of the observations. When phase-folding on the VSX period of 2.99250 days, the phase-folded light curve showed the dip broken up into three segments with no clear eclipse structure. When bRing data were phase-folded to 1.9952 days, two dips were recovered, but no clear eclipse structure was seen. Due to this lack of data in bRing, the period for this eclipsing system was not accurately determined.

HD 203244 was classified as an Algol eclipsing binary (EA) in both the VSX catalog and Rimoldini et al. (2012), with the latter reporting an unusually long period of 833.29734 days. We detect in the bRing photometry a very strong period at 12.77751 days; however, the phase-folded light curve at this period is shallow and does not show a secondary eclipse as expected from an EA. Phase-folding on the half or double period did not reveal additional structure. HD 203244 is most likely an ellipsoidal variable based on the period and shape of the phase-folded light curve.

4.2.2. New EBs

Three new EBs were identified and their phase-folded light curves are shown in Figure 5. To better identify the orbital periods for these new EBs, a BLS routine adopted from other works in this group was used (e.g., Talens et al. 2017a; Dorval et al. 2019).

HD 77669: this is a B9III/IV star (Houk 1978) with V magnitude 8.11 (Perryman & ESA 1997) and parallax $\varpi = 1.9553 \pm 0.0514$ mas, corresponding to distance $d = 511 \pm 13$ pc (*Gaia* DR2 5331845690580305920; Brown et al. 2018). We detect a strong period of 7.70766 days with a primary eclipse depth of 0.18 mag and a secondary eclipse depth of 0.15 mag. The observed transit depths in bRing are observed to be >0.15 mag; however, the bottom of the primary and secondary eclipses are too deep for bRing to accurately measure.

HD 142049 (HR 5900): HD 142049 is cataloged in VSX as a suspected variable (NSV 7318). The Washington Double Star catalog (Mason et al. 2019) reports HD 142049 as a 4.″8 binary with V magnitudes of 5.91 and 8.36, and the common motion and parallax of the pair is obvious in *Gaia* DR2 (*Gaia* DR2 5833110434699732352 and *Gaia* DR2 5833110434673386240; Brown et al. 2018). The *Gaia* DR2 parallaxes are 18.1136 ± 0.0678 mas and 18.1238 ± 0.0445 mas for A and B, respectively, showing the resolved pair to be at distance 55.2 pc. The spectral types of the components are a matter of some contention, with Houk & Cowley (1975) reporting components of type G5II/III and A3, noting that there is "*slight possibility there is a Am or Fm star component*," and Corbally (1984) reporting types of kA3hF3mF4 for the primary and F9.5V for the secondary. The bRing data show that the unresolved light from the system is consistent with a grazing EB with period 13.22062 day, with primary eclipse depth 0.050 mag and secondary eclipse depth of 0.045 mag. The binary must have a fairly eccentric orbit, as the eclipses are only 0.3 phase apart.

HD 155781: this $V = 7.43$ star has spectral type A3IV/V (Houk & Cowley 1975; Perryman & ESA 1997) and parallax 3.9861 ± 0.0561 mas, corresponding to distance $d = 250.9 \pm 3.5$ pc (*Gaia* DR2 5913908252773468928; Brown et al. 2018). We detect a strong signal at a period of 13.08670 days that appears to correspond to the orbital period of an EB with primary dips of 0.10 mag and secondary dips of 0.08 mag.

4.2.3. The O'Connell Effect

This survey searched for evidence of the O'Connell effect in all of the W UMa and β Lyr EBs in this data set. In W UMa and β Lyr EBs, the O'Connell effect is observed as an asymmetry in the maximum brightness in between the primary and secondary eclipses, i.e., the maximum before the primary eclipse is fainter than the maximum before the secondary eclipse (O'Connell 1951). The underlying physical mechanism is not well understood (plausible explanations include surface features and Doppler beaming: Wilsey & Beaky 2009; da Silva et al. 2014) though several examples have been detected (Pribulla et al. 2003, 2011; Burggraaff et al. 2018).

The O'Connell effect was detected in 18 of the bRing EBs, which have been tabulated in Table 4. The differences between the maxima were considered significant if they exceeded $3\sigma_A$, where σ_A is the uncertainty in the amplitude of the EB. Only two of the EBs in this table (TY Men (Nagy 1985; Pribulla et al. 2011) and TU Mus (Terrell et al. 2003) have been noted in the literature as having evidence of asymmetry in their light curves. The other 16 have likely been missed due to the faint effect observed in bRing and possible variability of the effect

Table 1
Previously Classified Cepheid Variables Detected with bRing

Name	HD	P	σ_P	A	σ_A	VSX ID	$P_{\rm VSX}$	V	SpT	References
⋯	⋯	(day)	(day)	(mmag)	(mmag)	⋯	(day)	(mag)	⋯	⋯
bet Dor	37350	9.844	0.007	157.8	1.6	13671	9.843	3.80	F6Ia	1
AP Pup	65592	5.085	0.003	127.8	2.6	26671	5.084	7.34	F8II	2
AX Vel	68556	2.592	0.001	82.8	1.5	37493	2.593	8.14	F6II	3
AH Vel	68808	4.229	0.033	87.5	1.2	37478	4.227	5.73	F7IB/II	3
RS Pup	68860	41.193	0.429	242.5	5.9	26613	41.443	7.00	F8Iab	2
V Car	72275	6.699	0.003	143.0	1.7	5758	6.697	7.30	F8Ib/II	1
RZ Vel	73502	20.482	0.067	264.4	4.0	37434	20.398	7.15	G1Ib	3
SW Vel	74712	23.381	0.067	251.7	3.9	37439	23.407	8.30	F8/G0Ib	3
SX Vel	74884	9.537	0.013	169.7	2.6	37440	9.550	8.34	F8II	3
BG Vel	78801	6.928	0.01	97.0	1.4	37501	6.924	7.68	F7/F8II	3
V Vel	81222	4.366	0.004	144.2	1.8	37421	4.371	7.57	F8II	1
I Car	84810	35.688	0.060	167.4	1.9	6330	35.552	3.74	G5Iab/Ib	1
V397 Car	87072	2.063	0.001	49.6	0.6	6150	2.063	8.30	F8IB/II	1
RY Vel	89841	27.952	0.177	201.2	3.2	37433	28.136	8.40	F5Ib/II	1
VY Car	93203	18.852	0.033	160.4	2.3	5796	18.890	7.62	F7Iab/Ib	1
U Car	95109	38.609	0.315	247.6	3.3	5757	38.829	6.45	G3Ia	1
ER Car	97082	7.722	0.011	103.0	1.4	5914	7.719	6.82	G1Iab/Ib	1
IT Car	97485	7.524	0.008	68.1	1.0	5990	7.533	8.11	F8Iab/b	1
V419 Cen	100148	5.502	0.005	61.7	1.0	7716	5.507	8.18	F7II	1
S Mus	106111	9.689	0.012	108.3	1.4	19678	9.660	6.08	F6Ib	1
R Cru	107805	5.818	0.004	140.4	2.1	10769	5.826	6.90	F7Ib/II	1
BG Cru	108968	3.345	0.002	45.4	0.6	10853	3.343	5.49	F5III	1
AG Cru	110258	3.836	0.004	89.5	1.5	10829	3.837	8.23	F8Ib/II	1
R Mus	110311	7.529	0.010	196.7	2.1	19677	7.510	7.51	F7Ib	1
S Cru	112044	4.687	0.001	146.9	2.0	10770	4.690	6.73	F7Ib/II	1
V659 Cen	117399	5.629	0.007	59.4	0.8	7956	5.623	6.65	F6/F7Ib	1
XX Cen	118769	10.938	0.021	171.5	2.4	7346	10.953	7.83	F7/F8II	1
V381 Cen	120400	5.080	0.002	151.2	2.1	7678	5.079	7.68	F8Ib/II	1
V Cen	127297	5.482	0.003	132.6	2.1	7302	5.494	6.80	F5Ia	1
AV Cir	130233	3.066	0.002	74.6	0.8	9474	3.065	7.44	F7II	1
AX Cir	130701	5.279	0.015	76.1	1.1	9476	5.273	5.94	F8II+A/F	1
⋯	132247[a]	2.123	0.008	8.7	0.2	412415	2.122	8.10	A0IV	3
R TrA	135592	3.392	0.002	129.8	1.3	36665	3.389	6.70	F7Ib/II	1
⋯	136633[a]	6.118	0.009	28.0	0.5	412524	6.125	8.21	B3V	1
LR TrA	137626	2.429	0.001	32.3	0.4	36930	2.428	7.79	F8II	1
S TrA	142941	6.324	0.006	162.3	1.8	36666	6.324	6.45	F8II	1
U TrA	143999	2.567	0.002	151.4	1.8	36668	2.568	7.92	F8Ib/II	1
S Nor	146323	9.754	0.018	84.1	1.0	19962	9.754	6.53	F8/G0Ib	1
RV Sco	153004	6.067	0.011	155.3	5.0	32830	6.061	7.16	G0Ib	2
V636 Sco	156979	6.803	0.010	93.5	1.5	33452	6.797	6.68	F7/F8Ib/II	3
V482 Sco	158443	4.529	0.007	106.0	3.5	33298	4.528	7.93	F8/G0II	2
V950 Sco	159654	3.378	0.001	67.0	1.1	33766	3.380	7.27	F5Ib	3
X Sgr	161592	7.018	0.003	278.0	8.6	27707	7.013	4.56	F7II	2
RY Sco	162102	20.063	0.007	172.8	5.1	32833	20.323	8.18	F6Ib	2
W Sgr	164975	7.597	0.001	172.4	6.9	27706	7.595	4.70	G0Ib/II	2
kap Pav	174694	9.031	0.008	180.9	2.1	25119	9.083	4.36	F5Ib-II:	1
XY Car	308149	12.430	0.055	5.5	0.1	5803	12.434	6.97	A9Ib-II	1

Note.
[a] Reclassified in this work, see Section 4.1.
References. (1) Houk & Cowley (1975), (2) Houk (1982), (3) Houk (1978).

(Wilsey & Beaky 2009) masking the asymmetry in previous studies.

4.3. δ Scuti Variables

We detected 66 δ Scuti variables in the bRing data set, 26 of which are candidates that had not been previously reported as detected pulsators. For the 40 previously known δ Scutis, we report only the strongest frequency in the bRing light curve. The previously published frequencies for the δ Scuti variables in Table 5 are from VSX by default; however, if one was not listed in VSX, we cite additional sources (Rodríguez et al. 2000; Rimoldini et al. 2012; Mellon et al. 2019a). The reported periods for 22 (55%) of the δ Scuti variables in Table 5 do not match those reported in previous studies. All of the δ Scutis are very tightly bound with their positions on the CMD (Figure 4; this is useful for confirming the new δ Scutis candidates by inspection. The bright δ Scuti variable β Pictoris itself was not included in this work because the bRing data for β Pictoris

Table 2
Previously Classified Eclipsing Binaries Detected with bRing

Name	HD	P (day)	σ_P (day)	A (mmag)	σ_A (mmag)	VSX ID	$P_{\rm VSX}$ (day)	V (mag)	SpT	References
zet Phe	6882	1.66985	1e-04	36.7	0.5	26329	1.66978	3.98	B6V+B0V	1
⋯	16589	6.33296	2e-04	5.4	0.2	53991	0.82414[a]	6.48	F6V	2
CN Hyi	17653	0.45609	2e-04	68.6	0.6	16473	0.45611	6.67	F6V	1
WZ Hor	17755	0.72886	1e-04	48.0	0.6	15947	0.72885	8.06	F3/F5V	1
VY Ret	21765	14.21605	5e-04	3.3	0.2	39786	14.21605	7.89	F5V	1
RZ Cae	29087	2.48712	5e-04	10.2	0.4	4529	2.48696	7.83	A4V	2
AN Dor	31407	2.03274	1e-04	13.2	0.3	13656	2.03268	7.67	B2/B3V	1
AR Dor	34349	2.95130	8e-05	4.7	0.1	13660	2.95206	7.03	F5V	1
UX Men	37513	4.18110	1e-03	25.5	0.8	18670	4.18110	8.25	F8V	1
TY Men	37909	0.46166	1e-04	99.0	1.0	18665	0.46167	8.26	A3/A4V	1
del Pic	42933	1.67248	2e-04	46.9	0.6	26396	1.67254	4.72	B0.5IV	1
V360 Pup	52993	1.12803	2e-04	10.7	0.3	26962	1.29644	6.57	ApSi	2
V361 Pup	54579	0.23661	5e-04	49.8	2.7	26963	0.36737	8.04	G0V	3
FF CMa	55173	1.21332	4e-04	67.2	3.2	5323	1.21337	7.48	B3/5V(p)	2
V452 Car	56146	2.11033	1e-05	23.2	0.4	6205	1.05502	8.10	B8IV	1
⋯	56910	1.83724	2e-05	5.7	0.2	55845	0.94929[a]	6.84	A2/3mA4-A7	1
V376 Pup	60559	3.88333	2e-04	3.8	0.2	26978	1.94270	6.25	B8IV(p Si)	2
V454 Car	60649	0.98049	1e-04	32.6	0.5	6207	0.98042	6.99	B4/B5V	1
V455 Car	61644	5.13038	2e-04	14.4	0.3	6208	5.13300	8.40	B5/B6IV	1
V606 Car	63203	12.31530	2e-03	9.5	0.4	42349	12.31920	8.31	B8/B9III	1
V397 Pup	63786	3.00402	2e-04	3.4	0.2	26999	3.00445	5.93	B9V	2
QZ Pup	64503	1.11207	2e-04	8.4	0.2	26936	1.11203	4.48	B2V	2
V Pup	65818	1.45441	2e-04	115.9	1.5	26607	1.45449	4.49	B1Vp+B2	4
⋯	66623	0.85182	1e-04	7.6	0.6	250227	0.42573	8.11	F7V	2
V462 Car	66768	1.10561	6e-05	30.7	0.4	6215	1.10569	6.71	B3V(n)	1
V431 Pup	69882	9.34999	1e-04	10.9	0.3	27033	9.35928	7.18	B1III:	5
⋯	70999	1.99520	5e-03	14.1	0.6	358580	2.99250	8.04	B3III	2
HR 3322	71302	4.93500	2e-04	4.4	0.2	27040	4.93500	5.97	B3V	5
NO Pup	71487	0.77183	2e-03	10.3	0.3	26892	1.25689	6.50	B9IV/V	2
XY Pyx	71801	0.92254	4e-04	10.1	0.4	27231	0.92254	5.74	B2V	2
X Car	72698	0.54132	1e-04	46.5	0.8	5760	1.08263	8.06	A0Vn	1
FY Vel	72754	33.88620	5e-04	39.2	0.6	37604	33.72000	6.89	B2Iape	5
V470 Car	72878	2.16177	2e-04	19.9	0.4	6223	2.16178	7.47	B9IV	1
V454 Vel	73699	1.13484	2e-04	16.1	0.4	272444	1.13492	7.58	B3V	2
NX Vel	73882	2.91834	3e-04	6.0	0.3	37715	2.91988	7.26	O8V:	6
RS Cha	75747	1.66999	1e-04	51.3	0.6	9248	1.66987	6.08	A7V	1
CV Vel	77464	6.89145	3e-04	2.1	0.1	37538	6.88949	6.70	B2V+B2V	5
GP Vel	77581	8.97155	2e-04	10.8	0.4	37614	8.964357	6.91	B0.5Ib	5
PQ Vel	78165	22.2632	1e-03	4.5	0.2	37731	22.2632	7.61	A2/3III(m)	5
V476 Car	78763	1.28135	2e-03	15.2	0.3	6229	1.28143	8.30	B7Vn	1
S Vel	82829	5.93101	2e-03	23.1	0.4	37418	5.93365	7.80	A5Ve+K5IIIe	7
IP Vel	84400	3.43679	1e-04	23.3	0.4	37649	3.43789	6.16	B6V	5
V486 Car	84416	1.09378	1e-04	32.7	0.4	6239	1.09389	6.32	A0V	1
KN Vel	85037	2.72327	1e-04	7.9	0.2	37663	2.72290	6.52	A2IV(m)	5
QX Vel	85185	0.87811	2e-04	37.8	0.6	37748	0.87807	8.00	A0V	5
QX Car	86118	4.47804	1e-04	14.0	0.3	6085	4.47804	6.66	B3V+B3V	1
V367 Car	86441	5.71172	2e-04	13.6	0.3	6120	5.73000	7.52	B6V	1
V341 Vel	89611	14.73000	9e-04	2.8	0.3	37757	14.73000	7.96	A0IV	5
V435 Vel	90000	10.49500	7e-04	4.7	0.2	37761	10.49500	7.56	B3V	5
⋯	90941	7.56760	4e-04	1.1	0.2	411431	7.56470	7.87	B4IV	5
CC Ant	91519	2.44594	6e-05	19.7	0.6	172655	2.44514	7.70	A8III	2
V661 Car	93130	0.39875	1e-04	14.8	0.4	56932	23.9438	8.08	O6III	6
RZ Cha	93486	2.83200	2e-04	24.8	0.4	9255	2.83208	8.08	F5V+F5	1
V356 Vel	93668	1.76804	2e-04	14.6	0.3	37772	1.76791	6.74	A0V	5
V772 Car	94924	0.88419	2e-04	27.4	0.4	172663	0.88417	8.01	A1V	1
V529 Car	95993	4.74574	2e-04	33.8	0.6	6282	4.74461	8.18	B8V	1
TU Mus	100213	1.38710	1e-04	101.9	1.3	19704	1.38728	8.40	O8(+O8)	6
V1101 Cen	102682	5.03350	2e-04	25.0	0.6	43976	5.03230	8.23	F5V	5
LZ Cen	102893	2.75772	1e-04	88.6	1.2	7571	2.75772	8.24	B2III	1
V788 Cen	105509	4.96697	1e-03	1.9	0.1	8085	4.96638	5.74	A3III	5
V831 Cen	114529	0.32142	5e-03	5.0	0.1	8128	0.64252	4.58	B8V	1
V964 Cen	115823	1.54308	1e-04	6.5	0.1	8261	1.54259	5.45	B6V	5
V979 Cen	119888	2.56882	7e-05	18.0	0.3	8276	2.56841	7.84	B8II	1

Table 2
(Continued)

Name	HD	P (day)	σ_P (day)	A (mmag)	σ_A (mmag)	VSX ID	P_{VSX} (day)	V (mag)	SpT	References
V1294 Cen	121291	1.16556	2e-04	25.4	0.5	45116	1.16553	7.89	A0Vn+K2(III)	5
AT Cir	122314	3.25748	3e-04	9.8	0.2	9472	3.25749	7.62	A5IV/Vs	1
V992 Cen	122844	1.21168	1e-04	16.4	0.3	8289	1.21156	6.20	A5III/IV	1
…	123720	0.86872	5e-05	16.4	0.3	58490	0.86880	7.75	A4V	1
V716 Cen	124195	1.49024	2e-04	32.9	0.5	8013	1.49010	6.09	B5V	8
RR Cen	124689	0.60570	1e-04	71.8	1.1	7307	0.60569	7.46	A9/F0V	1
…	129094	0.39881	2e-03	27.1	0.8	98784	0.74422	8.37	F7V	1
QZ Lup	131638	1.13658	1e-04	15.6	0.3	45479	1.13655	8.32	B9V	5
HR Lup	133880	1.75470	1e-04	11.9	0.3	17811	0.87748	5.76	B8IVSi	9
del Cir	135240	3.90445	1e-04	19.2	0.3	9529	3.90248	5.07	O8.5V	6
GG Lup	135876	1.84961	1e-03	4.9	0.3	17783	1.84961	5.59	B9V	5
MP TrA	143028	2.07017	3e-04	8.3	0.2	36942	2.06972	7.80	B7Ib/II	1
V399 Nor	147170	3.19301	3e-04	13.3	0.3	59034	3.19288	8.21	F6/F7V	3
V760 Sco	147683	1.73074	2e-04	15.1	0.6	33576	1.73090	7.05	B4V	2
OT Aps	148891	2.42603	9e-05	6.7	0.2	832	2.42660	8.00	B9.5IV	1
V1288 Sco	149450	1.10896	1e-05	32.0	0.6	46471	1.10890	8.23	B3III	5
V882 Ara	149668	20.96590	9e-05	4.3	0.2	59156	20.96590	7.61	A2IV	1
R Ara	149715	8.85166	2e-03	25.7	0.8	2804	4.42522	8.33	K0III	1
V954 Sco	149779	1.26883	1e-04	48.9	0.8	33770	1.26859	7.57	B2IV	5
V878 Ara	151475	0.77053	6e-05	46.0	0.7	136724	0.77046	8.05	B3II/III	5
V1290 Sco	151564	4.49267	2e-04	6.0	0.3	59217	4.49244	7.98	O9.5IV	5
HR 6247	151890	1.44647	1e-04	44.8	0.8	34007	1.44627	2.99	B1.5IV+B	10
V1295 Sco	152333	2.15767	3e-04	32.4	0.6	59262	2.15767	8.07	B1-2Ib-II	5
V861 Sco	152667	7.85382	1e-04	38.4	0.8	33677	7.84818	6.18	B0.5Ia	2
V883 Sco	152901	4.34113	1e-04	23.6	0.5	33699	4.34119	7.39	B2.5Vn	11
V836 Ara	153140	7.04075	2e-04	24.8	0.4	3639	7.03418	7.51	B1II	5
V616 Ara	154339	4.99671	6e-05	52.4	0.8	3419	4.99525	8.26	B3II/III	5
FV Sco	155550	5.72861	2e-04	37.9	1.4	33001	5.72790	8.07	B4IV	2
V1012 Sco	155775	1.51531	2e-04	12.0	0.2	33828	1.51548	6.72	B1V	6
V499 Sco	158155	2.33216	2e-04	67.2	2.5	33315	2.33330	8.29	B1III	2
V1081 Sco	158186	2.51419	1e-04	10.5	0.6	33897	2.51374	7.00	O9.5V(n)	6
V535 Ara	159441	0.31466	2e-04	30.2	0.4	3338	0.62930	7.36	A8V	1
V539 Ara	161783	3.16836	3e-04	19.6	0.3	3342	3.16909	5.70	B2V+B3V	1
V453 Sco	163181	12.00201	7e-05	82.7	2.4	33269	12.00597	6.60	O9.5Ia/ab	2
V1647 Sgr	163708	3.28277	1e-04	24.5	1.0	29347	3.28279	7.06	A3III	2
V2509 Sgr	167231	1.84197	4e-04	34.9	1.4	30209	1.08697	7.41	A0IV	2
V681 CrA	171577	4.32961	2e-04	2.8	0.2	10552	4.32788	7.74	B9V	5
V362 Pav	173344	2.74826	7e-05	5.3	0.1	25082	2.74844	7.39	A2mA5-A9	1
V363 Pav	174139	1.19491	1e-04	27.7	0.4	25083	1.19497	8.17	B9/B9.5V	1
V4407 Sgr	174632	1.45165	1e-04	19.1	0.8	32107	1.45174	6.64	B7/B8IV	8
…	177776	1.65022	7e-05	12.7	0.3	414518	1.65006	8.12	B9.5Vn	1
V4089 Sgr	184035	4.62891	3e-04	9.5	0.3	31789	4.62988	5.90	A5IV-III	5
HO Tel	187418	1.61294	2e-04	53.9	0.8	36458	1.61310	8.30	A7III(m)	5
V4437 Sgr	193174	1.13654	3e-04	36.0	1.3	32137	1.13662	7.24	A9IV/V	2
V386 Pav	198736	0.55187	2e-04	31.2	0.4	25106	0.55184	8.34	A9V	1
DE Mic	200670	0.20535	2e-04	16.6	0.5	137558	0.41069	7.80	F6/7V	2
BR Ind	201427	1.78553	2e-04	6.7	0.2	16577	0.89277	7.09	F8V	3
…	203244[b]	12.77751	7e-03	9.0	0.1	64006	833.29734[a]	6.98	G5V	3
CH Ind	204370	5.94788	2e-03	12.9	0.3	137591	5.95320	7.52	A9V	5
…	205877	7.68402	3e-04	7.4	0.1	64150	3.83266[a]	6.20	F7III	5
CP Gru	208614	2.08577	3e-04	29.1	0.4	14785	2.08615	7.72	A5V	5
DV Gru	210572	9.61553	1e-03	2.9	0.1	64287	4.81803	7.72	F8V	1
DK Tuc	212661	5.33386	4e-04	5.2	0.2	37084	5.33793	6.90	A1mA5-F0	1
DP Gru	220633	3.80231	3e-04	9.5	0.3	14807	3.80350	8.29	F5/F6V	5

Notes.
[a] Rimoldini et al. (2012).
[b] Reclassified.
References. (1) Houk & Cowley (1975), (2) Houk (1982), (3) Torres et al. (2006), (4) Hiltner et al. (1969), (5) Houk (1978), (6) Sota et al. (2014), (7) Sahade (1952), (8) Hube (1970), (9) Buscombe (1969), (10) Levato (1975), (11) Garrison et al. (1977).

Table 3
New Eclipsing Binaries Detected with bRing

HD	P	σ_P	Pri	Sec	VSX ID	V	SpT	References
⋯	(day)	(day)	(mag)	(mag)	⋯	(mag)	⋯	⋯
77669	7.70766	5e-04	0.180	0.15	⋯	8.10	B9III/IV	1
142049	13.22062	4e-05	0.050	0.045	45942	5.85	G5II/III+A3	2
155781	13.08670	6e-05	0.100	0.080	⋯	7.42	A3IV/V	2

References. (1) Houk (1978), (2) Houk & Cowley (1975).

Table 4
Eclipsing Binaries Showing the O'Connell Effect Detected with bRing

Name	A	σ_A	Max 1	Max 2	Δm
⋯	(mmag)	(mmag)	(mag)	(mag)	(mmag)
del Pic	46.9	0.6	4.6275	4.6301	2.6
V462 Car	30.7	0.4	6.5196	6.5120	7.6
TY Men	99.0	1.0	8.0567	8.0925	35.8
V535 Ara	30.2	0.4	7.3529	7.3551	2.2
V954 Sco	48.9	0.8	7.4828	7.4933	10.5
V772 Car	27.4	0.4	8.0544	8.0580	3.6
QZ Pup	8.4	0.2	4.4553	4.4584	3.1
DE Mic	16.6	0.5	7.7230	7.7323	9.3
HD 123720	16.4	0.3	7.7724	7.7772	4.8
LZ Cen	88.6	1.2	8.3148	8.3288	14.0
V979 Cen	18.0	0.3	7.4619	7.4654	3.5
V1012 Sco	12.0	0.2	6.6502	6.6525	2.3
V716 Cen	32.9	0.5	6.0115	6.0072	4.3
QX Vel	37.8	0.6	7.8886	7.8824	6.2
HR 6247	44.8	0.8	2.8767	2.8705	6.2
V470 Car	19.9	0.4	7.2323	7.2298	2.5
TU Mus	101.9	1.3	8.2469	8.2266	20.4
RR Cen	71.8	1.1	7.2808	7.2752	5.6

were recently published and analyzed in Zwintz et al. (2019). The mismatches may be due to a variety of reasons, including aliasing or the presence of multiple modes; however, the star θ Tuc had an additional feature in its periodogram that is not δ Scuti in nature.

HD 3112 (θ Tuc): θ Tuc is a well-studied δ Scuti that is also a well-studied binary system (e.g., Cousins & Lagerweij 1971; Stobie & Shobbrook 1976; Kurtz 1980; Bos 1994; Sterken 1997; De Mey et al. 1998). The primary pulsation reported in the VSX catalog is 20.28068 day^{-1}, which agrees with prior observations (Cousins & Lagerweij 1971; Stobie & Shobbrook 1976; Kurtz 1980; Liakos & Niarchos 2017). However, the dominant period detected by bRing is 0.28165 day^{-1}, which is reported in Table 5. This pulsation has been previously identified as orbital motion associated with the binary nature of the system (0.281 day^{-1}: Sterken 1997; De Mey et al. 1998). A search of the bRing periodogram around the expected δ Scuti frequencies recovers a primary δ Scuti frequency of 17.06312 day^{-1}.

The 26 new candidate δ Scuti variables all had faint primary pulsation amplitudes of $<$10.5 mmag, with the exception of HD 216743, and they all had brightnesses in the range $V \simeq$ 6.5–8.3, and are reported in Table 6 (showing the primary pulsation frequency as seen by bRing). Most of the newly discovered δ Scuti variables in the bRing survey were in the faint end of the magnitude range for the instrument ($V < 6.5$); the two brighter candidates were HD 171819 ($V = 5.84$) and HD 189951 ($V = 5.25$) (Kharchenko & Roeser 2009). Further analysis of the frequencies detected with the bRing time-series photometry for the previously discovered and newly discovered δ Scuti variables is encouraged and out of the scope of this work.

The star HD 140566 (included in Table 7) was labeled as detached EB by the VSX with a period 193.70000 days. bRing detected a much shorter period at 0.08783 days (11.38563 day^{-1}). This star is poorly studied with no prior follow-up work attempting to confirm the nature of this variable. The bRing period and light curve are not indicative of an eclipsing system. The combination of the detected pulsation in the bRing light curve and the star's spectral type (A5IV) indicate that the star is likely to be a δ Scuti variable. This agrees with its position among other δ Scutis in the CMD from Figure 4 ($(B-V)_0 = 0.16$, $M_V = 0.99$). Therefore, this star is not an eclipsing system and is reclassified in this work as a candidate δ Scuti.

4.4. Other Variables

In addition to the variables discussed in the previous sections, bRing detected evidence of periodic pulsations representing several different "other" classes of variability including ellipsoidal variables (ELLs), rotation periods (ROT), and β Cepheids (BCEPs), among others. bRing was particularly sensitive to low-amplitude (typically $\simeq$ 10 mmag) slowly pulsating B stars (SPBs) and LPVs. In Table 7, we list 80 stars previously classified as variables in the VSX catalog, along with their VSX and bRing variability parameters, and classification in the VSX catalog (last column). We discuss some of these stars further in Section 4.4.1 if the period of a non-LPV star detected with bRing was significantly different than a previously published period or if the periodogram revealed new additional periods of interest. In Table 8, a list of new period detections or variable classifications is provided for 25 stars using this system based on their spectral and pulsation properties and light-curve shapes, and these stars are discussed further in Section 4.4.2.

4.4.1. Previously Known Variables

In comparing the periods determined using bRing data to those listed in either VSX or Rimoldini et al. (2012), we find that only 20 of the 80 (25%) had completely different periods. We discuss the ones that showed period differences in this section.

bRing was able to provide more precise period measurements for five of the LPV, SR, and SRD stars. Five of these stars had completely different periods from the low-precision periods reported in VSX or Rimoldini et al. (2012).

HD 177171 (ρ Tel): for the young F5V HD 177171, we detect a strong periodicity of 1.55258 days. However, Rimoldini et al. (2012) quote a period of 0.71187 day, and VSX reports a period of 4.73687 days from Koen & Eyer (2002). Both estimates are based on the sparse *Hipparcos* time-series photometry (~70 data points),

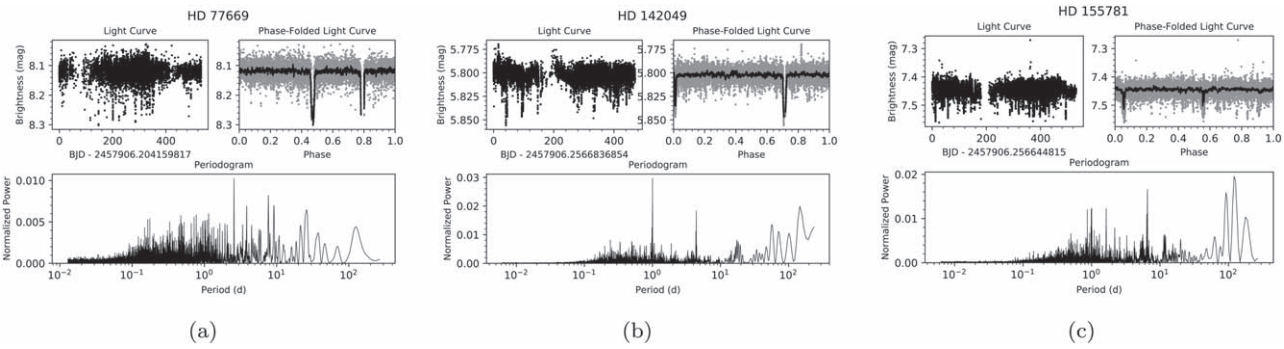

Figure 5. Light curves, periodograms, and phase-folded light curves of the three new eclipsing binaries detected in this survey.

Table 5
Previously Classified δ Scutis Detected with bRing

Name	HD	f (day^{-1})	σ_f (day^{-1})	A (mmag)	σ_A (mmag)	VSX ID	$f_{\rm VSX}$ (day^{-1})	V (mag)	SpT	References
θ Tuc	3112	0.28165	2e-04	4.0	0.2	37102	20.28068	6.11	kA7hA7mF0(IV)	1
⋯	8351	14.13144	5e-05	3.7	0.2	53727	14.06695[a]	6.70	A9V	2
BD Phe	11413	27.02703	4e-03	4.9	0.2	26294	25.21158[a]	5.93	A1Va λ Boo	3
⋯	12284	6.25500	7e-05	5.2	0.3	53855	6.20694	7.68	A9III	2
RX Cae	28837	8.27307	5e-04	6.5	0.3	4527	6.48925	7.01	F3/F5II	4
X Cae	32846	0.29564	1e-04	5.0	0.3	4518	0.27049	6.31	F2IV/V	2
YY Pic	39244	18.51316	3e-04	3.7	0.2	26385	9.73985	7.79	A7V	4
⋯	41846	10.47770	4e-05	5.3	0.2	⋯	10.33475[a]	8.12	A6mA7-F0	5
⋯	46586	14.82017	5e-04	2.9	0.2	410727	14.82052	8.04	F0III	4
V638 Pup	58635	8.66695	5e-03	2.5	0.1	26970	8.66699	6.82	A8V	2
V393 Car	66260	14.1551	1e-04	6.8	0.2	6146	7.07741	7.47	A7III/IV	5
AI Vel	69213	11.59990	1e-04	49.0	0.9	37479	8.96265	6.56	A9IV-V	4
OX Vel	77347	12.60254	1e-04	11.5	0.2	37727	12.60255	7.58	A4mA7-A9	5
ER Cha	88278	14.27857	1e-04	3.9	0.1	9398	15.72376	7.31	A3/5III/IV	5
LW Vel	88824	12.58582	5e-05	3.8	0.1	37687	8.98093	5.27	F0Vn	1
⋯	90611	15.19447	4e-04	2.5	0.2	⋯	15.19498[a]	6.55	F0IV/V	4
IW Vel	94985	10.14809	2e-04	4.3	0.1	37656	6.66666	5.90	A4V	4
V1023 Cen	102541	19.89813	5e-03	4.1	0.2	8320	20.00000[b]	7.95	hF0VkA5mA5 λ Boo	6
EE Cha	104036	33.86956	3e-04	3.4	0.1	9386	33.33333[b]	6.73	A7V	5
⋯	111984	23.49741	5e-05	3.3	0.1	⋯	21.46347[a]	7.28	A5V	4
V853 Cen	126859	16.30857	8e-04	2.4	0.3	8150	18.92013	6.97	A6V	5
IN Lup	142994	9.16564	6e-05	3.0	0.2	17824	7.87402[b]	7.17	F2VkA3mA3 λ Boo?	7
IO Lup	143232	13.40241	5e-04	3.0	0.1	17825	15.59193[a]	6.67	kA7hA5mF2	8
V922 Sco	153747	23.80734	1e-03	2.7	0.2	33738	20.00000	7.40	hA7VmA0 λ Boo	6
⋯	156623	71.14754	8e-04	3.4	0.1	⋯	71.14300[c]	7.24	A1V PHL	6
⋯	157321	10.51587	2e-05	9.7	0.2	60284	10.51640	8.02	A9IV/V	5
V703 Sco	160589	6.66876	6e-04	25.2	1.4	33519	8.67922	7.85	F0V	6
V346 Pav	168740	12.57296	1e-04	2.6	0.1	25066	16.98244[d]	6.12	A8VkA2mA2 λ Boo	7
V353 Tel	173794	0.61578	3e-04	4.7	0.1	137348	0.31250	7.11	A3III/IV	4
QQ Tel	185139	8.41297	3e-04	4.3	0.1	36568	15.38462	6.26	F2IV	4
⋯	192316	33.0221	1e-03	3.4	0.2	⋯	22.80867[a]	7.55	A8V	5
⋯	198592	26.34244	8e-04	2.7	0.3	⋯	21.59235[a]	7.58	A3III	4
⋯	200475	1.11423	2e-05	9.5	0.2	305774	1.11499	7.82	A3mA5-A7	5
⋯	201292	14.7769	4e-05	5.2	0.2	⋯	25.80477[a]	8.19	A3II	5
CK Ind	209295	1.12963	3e-04	25.3	0.3	137616	1.12934	7.32	A9/F0V	5
DR Gru	213669	14.01768	7e-05	7.6	0.2	137628	15.01502	7.41	F0VkA2.5mA2.5 λ Boo	7
⋯	218090	1.81606	1e-04	6.3	0.1	305852	1.81590	8.13	F0V	5
⋯	219301	9.28928	3e-05	3.6	0.2	250337	9.28966[a]	6.56	F0III	5
RS Gru	⋯	13.60412	6e-05	46.9	0.7	14680	6.80218	8.27	A9IV	4
HIP 35815	⋯	7.70897	5e-05	6.9	0.3	55889	10.83677[a]	7.84	F0	9

Notes.
[a] Rimoldini et al. (2012).
[b] Rodríguez et al. (2000).
[c] Mellon et al. (2019a).
[d] Paunzen et al. (1998).

References. (1) Gray & Garrison (1989), (2) Houk (1982), (3) Gray & Garrison (1987), (4) Houk (1978), (5) Houk & Cowley (1975), (6) Paunzen et al. (2001), (7) Gray et al. (2017), (8) Paunzen & Duffee (1996), (9) Boss (1937).

Table 6
New Candidate δ Scutis Detected with bRing

HD	f	σ_f	A	σ_A	VSX ID	V	SpT	References
⋯	(day^{-1})	(day^{-1})	(mmag)	(mmag)	⋯	(mag)	⋯	⋯
3463	10.50785	5e-04	3.7	0.2	⋯	8.04	A6/8V	1
20232	45.45826	2e-04	2.1	0.2	⋯	6.88	A2/A3III/IV	2
25860	15.34882	4e-04	2.0	0.1	⋯	6.62	A4/A5IV	1
43898	19.31816	2e-04	2.6	0.3	⋯	7.87	A8/A9V	2
46978	16.6692	2e-03	4.4	0.2	⋯	8.16	A6V	1
57969	68.46621	5e-03	2.1	0.1	55878	6.56	A1V	1
72979	10.49512	8e-04	6.0	0.1	⋯	7.70	A4Vs	1
81771	11.81314	4e-04	3.6	0.1	⋯	7.76	A4V	1
82484	4.53561	8e-03	7.2	0.3	⋯	8.09	A3III/IV	2
92762	16.39493	8e-04	4.1	0.2	⋯	7.80	A8V	1
110080	18.55808	6e-04	2.7	0.1	⋯	7.41	A5V	1
121191	21.59957	3e-03	7.7	0.2	⋯	8.16	A5IV/V	3
156408	10.64459	3e-04	10.4	0.3	33894	8.27	A7V	2
163482	5.92257	3e-03	3.0	0.1	274692	6.82	A0III/IV	2
168651	15.66042	3e-04	2.5	0.2	⋯	7.40	A9III	3
170461	12.59065	5e-04	3.7	0.2	250253	6.98	A9IV	2
171819	13.55119	2e-04	2.4	0.3	⋯	5.84	A7IV/V	3
172995	13.17514	2e-04	3.3	0.1	⋯	6.81	A9IV	3
177523	13.11519	2e-04	2.6	0.2	⋯	7.49	A9/F0IV	3
177665	11.34302	2e-04	5.1	0.2	⋯	8.37	F2IV	3
189951	12.19356	5e-04	2.1	0.3	63419	5.25	A9IV	3
191585	15.46432	4e-04	4.4	0.1	⋯	6.92	A2/3IV	2
200203	19.31605	7e-04	2.1	0.3	⋯	7.35	A4/A5II/III	1
204352	14.35455	3e-05	2.9	0.2	⋯	8.40	A9V	1
208094	18.46880	4e-04	3.0	0.3	⋯	8.21	A2IV	1
216743	16.88458	3e-04	43.3	0.2	⋯	7.25	A3V	3

References. (1) Houk & Cowley (1975), (2) Houk (1982), (3) Houk (1978).

whereas the bRing data set has $>10^2$ more points and dense coverage. We do not detect significant peaks at the periods reported by either Rimoldini et al. (2012) or Koen & Eyer (2002) (in VSX).

HD 60168 (PS Pup): with bRing we detected a slightly different period (2.07742 days) for the ELL variable PS Pup compared to that published in VSX (1.34220 days). The periodogram for PS Pup does not have a significant period near the VSX period of 1.34220 days and the detected bRing period is near the 2 day alias of the sidereal systematic. The star and its periodicity detected with bRing are reported in Table 7 because the expected shape of an ELL variable is recovered at this period versus the sinusoid expected from a sidereal alias (hence we believe the periodicity to be real).

HD 172416 and HD 189631: the γ Dor-type stars HD 172416 and HD 189631 both had different periods in bRing than they have reported in VSX. For HD 172416, the reported VSX period is 0.99787 day, which is close to the primary sidereal systematic. If this was a real signal in bRing, it could not be recovered due to the proximity to this dominant systematic. The 0.59900 day signal for HD 172416 was not recovered at all in the bRing periodogram and the detrending routine should not affect this period. The periodogram for this star revealed the primary period of 0.70578 day, as well as additional significant periods that could be useful for future analysis.

V946 Cen, HD 116862, and V846 Ara: there were several Be stars detected by bRing. bRing measured a different period for the stars V946 Cen, HD 116862, and V846 Ara compared to that reported in VSX; these three stars also happen to be γ Cas (GCAS) variables, which are known to be irregularly variable on the order of a decade. The time between the study of Rimoldini et al. (2012) and bRing (~5–7 yr) could be enough time for periods to drift, causing the differences in observed periods. bRing's long baseline could also be a factor, picking up underlying shifts. In particular, V946 Cen and HD 116862 both show two dominant periods, while V846 Ara only shows a single dominant period at 0.43861 day.

The RS CVn (RS) variables hosted the most discrepancies between observed bRing periods and prior studies. bRing detected completely different periods for ρ Tel, HD 201247, and HD 209234; bRing detected near half the original period for HD 56142.

bRing detected 26 slowly pulsating B-type (SPB) stars (including 4 new ones from Section 4.4.2 and the reclassified classical Cepheid HD 136633 from Section 4.1). These stars are characterized by their spectral type, location near the main-sequence (as observed for this sample in Figure 4), and periods ranging from just short of a day to several days (De Cat 2007; Miglio et al. 2007). They are also known to exhibit multiple oscillations in their light curves (Miglio et al. 2007) and have even coexhibited BCEP pulsations in a few rare cases (De Cat 2007).

The periodograms for all of the SPB variables were individually inspected for multiple periods or shorter periods that may indicate BCEP pulsations similar to the stars from (De Cat 2007). In general, the previously observed SPB variables showed multiple independent periods in their periodograms and bRing detected different primary periods for HD 85871 and HD 159041. Further analysis of the SPB stars detected with bRing is beyond the scope of this work.

Table 7
Other Previously Classified Variables Detected with bRing

Name	HD	P	σ_P	A	σ_A	VSX ID	$P_{\rm VSX}$	V	SpT	References	Type
⋯	⋯	(day)	(day)	(mmag)	(mmag)	⋯	(day)	(mag)	⋯	⋯	(VSX)
⋯	13397	48.32756	4e-02	10	0.2	280885	49.20000	7.74	K0III	1	ROT
UX For	17084	0.95197	1e-03	21.3	0.5	14260	0.95600	8.04	G5/8V+(G)	2	RS
TV Pic	30861	0.85175	3e-05	30.1	0.4	26362	0.85199	7.44	A2V	1	ELL
TU Pic	33331	1.14708	2e-04	9.0	0.2	26361	1.14686	6.90	B5III	1	SPB
R Pic	30551	141.89257	26e00	523.7	5.4	26334	168.00000	7.59	K2/K3II:pe	1	SR
YZ Men	34802	19.36778	8e-02	24.1	0.3	18686	19.58000	7.76	K1IIIp	3	RS
AB Dor	36705	0.51443	2e-04	10.6	0.2	13645	0.513900	6.93	K1III(p)	3	TTS/ROT
lam Col	39764	1.28660	1e-03	1.4	0.3	9602	1.28701	4.87	B5V	2	ELL
SZ Pic	39917	4.94895	4e-03	0.1	0.4	26359	4.95000	7.89	G8V	2	ELL
TY Pic	42504	48.82267	3e-01	7.8	0.3	26365	50.20000	7.70	G8/K0III+F	3	RS
V Pic	43518	166.32289	2e00	16.8	0.2	26338	180.00000	7.41	K2III	3	SR
AE Men	46291	12.14125	2e-02	13.9	0.2	18692	12.03000	8.25	K2III+F/G	3	RS
TZ Pic	46697	13.64700	3e-03	13.7	0.2	26366	13.68000	7.64	K1III/IVp	3	RS
V448 Car	49877	55.99252	1e-01	49.8	0.5	6201	⋯	5.61	K5III	3	SRD
⋯	56142	10.57968	4e-01	6.1	0.3	55829	21.16000	7.57	F6/F7V	2	RS
PS Pup	60168	2.07742	2e-03	8.1	0.4	26919	1.34220	6.62	B8V	2	ELL
V372 Car	64722	0.11540	1e-05	4.6	0.1	6125	0.11600	5.68	B1.5IV	3	BCEP
V413 Pup	66235	1.59433	9e-04	11.1	0.3	27015	1.59406	7.68	B9IV	1	SPB
V415 Pup	66503	0.84905	1e-04	7.5	0.2	27017	0.84892	8.22	B5V	1	SPB
QR Pup	69342	3.55155	7e-04	21.5	0.4	26928	3.55180	8.06	B3II	1	ELL
HV Vel	73340	2.66807	8e-04	6.2	0.1	37638	2.66745	5.78	ApSi	1	roAp
omi Vel	74195	2.79716	1e-03	7.3	0.2	37807	2.79759	3.59	B3IV	1	SPB
⋯	74422	0.74500	0.001	42.4	0.5	400557	0.74500	8.12	A3IV	3	ACEP
V473 Car	76640	0.95421	1e-04	8.1	0.1	6226	0.95399	6.35	B5V	3	SPB
OW Vel	76875	66.50249	2e+00	51.7	0.6	37726	64.54000	7.66	K2/3III+A/F	1	SRD
OY Vel	77653	1.48775	4e-04	6.6	0.1	37728	1.48782	5.03	B9	1	ACV
PR Vel	78405	1.23898	4e-04	10.6	0.3	37732	1.23890	8.26	B5IV	1	SPB
PS Vel	79039	1.07481	1e-04	9.4	0.2	37733	1.07460	6.82	B4V	1	SPB
V480 Car	81654	40.80297	5e-01	18.9	0.5	6233	40.00369[a]	7.87	B2/3V(e)	3	BE + GCAS
QZ Vel	85871	5.71790	7e-03	5.2	0.2	37750	1.03108	6.49	B1V	3	SPB
V335 Vel	85953	3.75717	3e-03	6.1	0.1	37751	3.75520	5.94	B2V	4	SPB
⋯	88825	1.45753	3e-05	10.5	0.2	⋯	⋯	6.09	B4Ve	3	BE(SPB)
V514 Car	92287	2.90561	6e-04	3.8	0.1	6267	2.90457	5.88	B3IV	3	ELL
V431 Car	97152	1.61853	1e-05	6.7	0.2	6184	1.61853	8.07	WC7+O7V	5	E/WR
KQ Mus	100359	1.23848	3e-04	13.6	0.2	19926	1.23834	6.88	B7IV	3	SPB
V810 Cen	101947	151.28362	7e-01	16.0	0.2	8107	130.00000	5.01	F9Ia	6	LPV
DE Cru	104631	3.68406	3e-03	10.2	0.2	10896	3.68800	6.77	B1II	3	SPB
DF Cru	104705	1.13486	2e-04	13.8	0.2	10897	1.13480	7.81	B0.5III	3	SPB
V1123 Cen	108015	58.59871	1e+00	42.5	0.6	44225	60.60000	7.97	F3/5Ib/II	1	SRD
V946 Cen	112999	1.13651	1e-04	12.2	0.2	8243	0.08883[a]	7.38	B6III(n)	7	BE+GCAS
⋯	116862	0.80112	7e-04	3.7	0.1	58241	2.87078[a]	6.26	B3IV	1	BE+GCAS
⋯	118258	49.69547	1e+00	4.8	0.2	287154	50.50000	8.01	G6V	3	RS
DF Cir	124672	0.36907	1e-05	13.7	0.2	136640	0.367772	7.55	F6V	8	ELL
V1001 Cen	125104	6.73825	1e-02	10.1	0.3	8298	6.73600	7.29	B4IV/V	3	DPV/ELL
HX Lup	125721	3.08809	7e-04	5.0	0.1	17817	3.08809	6.11	B1III	1	ELL
V761 Cen	125823	8.81327	2e-02	6.5	0.3	8058	8.81710	4.41	B2V	2	SXARI
eta Cen	127972	0.64250	6e-05	7.9	0.3	8347	0.64247	2.33	B1Vn+A	9	GCAS+LERI
LS TrA	137164	44.46069	6e-01	39.9	0.4	36931	45.00000	7.47	K1/K2IVp	3	RS
HV Lup	137518	2.82838	2e-03	38.9	0.7	17815	⋯	7.74	B1/2(I/IIIN)	9	BE
LZ TrA	138521	0.57015	6e-05	7.4	0.2	36938	0.57019	8.04	B9IV	3	SPB
⋯	140566[b]	0.08783	1e-05	3.3	0.2	415978	193.70000	8.28	A5IV	1	ESD(DSCT)
⋯	142542	92.14955	2e+00	4.1	0.2	412695	324.00000	6.29	F3/F5V	2	M
V374 Nor	147894	2.77589	3e-04	6.7	0.2	20334	2.72950	7.24	B5III	1	ELL
V918 Sco	149404	9.81300	5e-03	4.8	0.1	33734	9.81300	5.48	O9Ia	10	ELL
⋯	149455	1.28303	2e-04	6.8	0.2	59146	1.28217	7.69	B7III/IV	3	SPB
⋯	151158	0.18178	1e-05	6.3	0.2	225575	0.18178	8.21	B2Ib/II	1	BCEP
OV Aps	151665	0.92038	1e-04	9.7	0.2	834	0.92044	8.07	A7III	3	ACV
V846 Ara	152478	0.43861	2e-05	8.0	0.2	3649	0.60646[a]	6.30	B3Vnpe	9	BE+GCAS
V847 Ara	152511	0.94205	1e-04	6.5	0.1	3650	0.94213	6.53	B5III	3	SPB
V884 Sco	153919	3.41141	4e-04	7.3	0.2	33700	3.41161	6.53	O5F	10	ELL+HMXB
⋯	155190	1.66574	7e-04	7.2	0.1	59550	1.66571[a]	7.12	B7III/IV	3	SPB
V824 Ara	155555	1.68379	5e-05	6.5	0.1	3627	1.68160	6.87	K1Vp	3	RS

Table 7
(Continued)

Name	HD	P (day)	σ_P (day)	A (mmag)	σ_A (mmag)	VSX ID	P_{VSX} (day)	V (mag)	SpT	References	Type (VSX)
⋯	156853	1.15959	3e-04	4.1	0.1	⋯	1.15945	7.60	AP SI	1	ACV
⋯	159041	3.80296	3e-03	5.9	0.2	⋯	0.09432[a]	8.04	B9Ib/II	1	SPB
V1092 Sco	163254	0.83175	2e-04	11.2	0.2	33908	0.83167	6.74	B5Vn	1	SPB
V692 CrA	166596	1.65010	3e-02	4.1	0.2	10563	1.67000	5.46	B2.5III	1	SXARI
⋯	172416	0.82698	3e-04	6.6	0.1	62979	0.99787	6.61	F5V	1	GDOR
V364 Pav	175008	0.57389	5e-05	6.6	0.1	25084	0.57389	6.80	B9IV/V	3	SPB
rho Tel	177171	1.55272	6e-05	4.7	0.1	63113	4.73687	5.17	F7V	1	RS
⋯	189631	0.70578	8e-05	6.8	0.2	63407	0.59900	7.54	A9V	1	GDOR
⋯	193677	0.42930	3e-03	3.2	0.1	281860	0.85857	7.60	A2V	3	ROT
⋯	201247	6.32432	2e-02	2.7	0.1	63923	1.26590[a]	6.84	G0	11	RS
⋯	209234	4.67895	1e-01	4.6	0.1	⋯	0.089454[a]	7.87	G3V	8	RS
CX Gru	214291	0.87089	1e-04	11.7	0.2	14793	0.87125	6.57	F7V	1	ELL
ksi Oct	215573	1.76908	3e-04	5.7	0.1	20485	1.76866	5.32	B6IV	5	SPB
⋯	216668	1.78959	4e-04	6.2	0.2	305847	1.78997	7.89	A1V	3	VAR
BP Gru	217522	0.18301	2e-02	1.7	0.1	14762	⋯	7.52	Ap(Si)CR	12	roAp
CF Oct	196818	20.46033	3e-02	20.4	0.3	20449	19.97000	7.90	K0IIIp	3	BY
SX Phe	223065	0.05496	6e-03	33.4	0.8	26236	0.05496	7.31	A2Vvar	1	SXPHE
V715 CrA	168403	4.80085	3e-03	13.8	0.2	10586	4.79920	6.78	A0II/III(p)	2	ACV

Notes. ACEP: anomalous Cepheid. ACV: α^2 CVn. BCEP: β Cephei. BE: Be star. BY: BY-Draconis type. DPV: double periodic. DSCT: δ Scuti. ED/ESD: detached EB. ELL: ellipsoidal variable. GCAS: γ Cass-type. GDOR: γ Dor-type. HMXB: high-mass X-ray binary. LERI: λ Eri-type. LPV: long period. M: Mira-type. roAp: chemically peculiar, rapidly oscillating A star. RS: RS CV-type. SDOR: S Doradus-type. SPB: slowly pulsating B-type. SXARI: SX Arietis-type. SXPHE: SXPHE-type variable. TTS: T Tauri Star. WR: Wolf–Rayet.
[a] Rimoldini et al. (2012).
[b] Reclassified.
References. (1) Houk (1978), (2) Houk (1982), (3) Houk & Cowley (1975), (4) Cucchiaro et al. (1977), (5) Shara et al. (2009), (6) Keenan & McNeil (1989), (7) Garrison et al. (1977), (8) Torres et al. (2006), (9) Levenhagen & Leister (2006), (10) Sota et al. (2014), (11) Gray et al. (2006), (12) Levato et al. (1996).

HD 140566: the final star that showed a different period than the reported VSX period was HD 140566 (previously discussed in Section 4.3). bRing detects a period at 0.08783 days, whereas VSX reports a 193.7000 day period and classified the star as a detached EB (ESD). The bRing light curve does not indicate evidence of an eclipsing system. The period is more indicative of a δ Scuti, and multiple modes appear in the periodogram. Its spectral type (A5IV) and CMD position (from Figure 4) agree with a δ Scuti classification. Therefore, this star should be relabeled as a candidate δ Scuti.

4.4.2. New Variables

In Table 8, we list 25 stars that had no known previously published periodicity or classification. A suggested classification was based on the period of the activity, the shape of the light curve, and the spectral type of the star.

The stars HD 103285, HD 73141, and HD 99757 were classified as SPB variables based on their periods and locations in Figure 4. The star HD 76566 (IY Vel) was also observed by Lefèvre et al. (2009), which also detected the 2.10650 day period. However, they left the SPB classification as uncertain; the SPB nature of this star is confirmed with the bRing data. Due to bRing's long baseline, it was possible to detect several long-period variables out to the Nyquist limit of the observations (typically around 266 days). The population of these variables is composed largely of K giants. For the stars in Table 8, the survey was able to either provide newly measured periods or provide more precise values over VSX periods.

HD 143098: for the G5V star HD 143098, a 8.56567 day period was detected that is indicative of rotation. The star also shows enhanced chromospheric activity ($\log R'HK = -4.46$, -4.59 Boro Saikia et al. 2018) and strong Li I absorption (EW (Li I λ6707 $= 60$ mÅ; Torres et al. 2006). Combining this ROT with the $B - V$ color (0.686 ± 0.015) reported in *Hipparcos* (Perryman & ESA 1997), and the age-rotation calibration of Mamajek & Hillenbrand (2008), we estimate a gyrochronological age of HD 143098 of 0.6 Gyr. This is consistent with the other two indicators—both the Li absorption strength and the chromospheric activity are also very consistent with an age similar to that of the ∼0.6–0.8 Gyr old Hyades (Soderblom 1990; Mamajek & Hillenbrand 2008).

4.5. Irregular Variables

We also detected 17 irregular variables with the bRing photometry, which are listed in Table 9. The table includes previously known irregular variables (Be stars, Mira variables) as well as stars whose bRing light curves showed evidence of variability, but for which no significant period could be converged on.

The majority of these irregular variables exhibited very short bright events (HD 3359, HD 68809, HD 69256, HD 72838, HD 91869, HD 127755, HD 128679, HD 205834). These events were only a few hours in nature and could be degenerate with isolated stochastic events in the bRing data.

The light curve for HD 92063 shows three consecutive bumps in the brightness that extend as bright as 0.3 mag. The source of the bumps is likely due to the effects of the nova ASASSN-18fv (Nova Carina 2018, V906 Car) (Stanek et al. 2018), situated only 128″ away from HD 92063. ASASSN-18fv was alternatively classified as either a classical nova

Table 8
Other New Variables Detected with bRing

Name	HD	P (day)	σ_P (day)	A (mmag)	σ_A (mmag)	VSX ID	P_{VSX} (day)	V (mag)	SpT	References	Type (VSX)
⋯	4737	82.79415	4e00	5.1	0.1	⋯	⋯	6.27	G8III	1	LPV
⋯	5135	51.35633	3e-01	6.5	0.2	⋯	⋯	7.87	G3IV/V	1	LPV
⋯	6269	99.68567	9e00	13.4	0.8	⋯	⋯	6.28	G8IIICN...	2	LPV
⋯	11597	72.28817	4e00	20.7	1.1	⋯	⋯	8.15	F5V	2	LPV
⋯	32453	29.02423	4e-01	3.9	0.1	⋯	⋯	6.01	G8III	2	LPV
⋯	39937	47.04209	0.39153	10.4	0.2	41338	⋯	5.94	F7IV	3	LPV
⋯	53143	9.59515	6e-02	8.5	0.1	⋯	⋯	6.81	K0IV-V	3	ROT?
f Pup	61330	85.64948	1e-02	5.2	0.2	⋯	⋯	4.53	B8IV/V	2	LPV
⋯	73141	0.89316	2e-04	12.5	0.3	⋯	⋯	8.40	B7 III/IV	1	SPB
⋯	76006	17.97482	1e-01	4.0	0.1	⋯	⋯	7.32	F5/6 III	1	LPV
IY Vel	76566	2.10650	2e-03	3.6	0.1	37658	⋯	6.25	B3IV	1	SPB
⋯	87896	58.02840	1e00	6.2	0.1	⋯	⋯	6.91	G8III	3	LPV
⋯	90885	7.83318	3e-01	3.8	0.1	⋯	⋯	8.33	K2/K3III	4	ROT?
⋯	99757	1.13729	4e-04	12.5	0.3	⋯	⋯	8.16	B7 II/III	1	SPB
⋯	103285	1.33863	1e-04	6.6	0.3	411690	164.30000	8.23	B9.5V	3	SPB
⋯	129118	72.74121	14e00	5.4	0.1	⋯	⋯	6.79	K0III	1	LPV
KL Lup	135411	65.04632	26e00	15.5	0.4	17838	⋯	8.24	K5III	2	LPV
⋯	143098	8.56567	3e-04	3.5	0.2	⋯	⋯	7.64	G5V	4	ROT
⋯	144951	114.70571	2e-01	21.0	0.3	412789	138.00000	8.06	B3 V	3	LPV
⋯	149238	139.28268	6e00	32.5	0.3	36806	299.00000	8.04	F8V	3	LPV
⋯	156768	121.17629	6e00	4.7	0.1	⋯	⋯	5.86	G8Ib/II	3	LPV
⋯	167714	147.74923	24e00	5.0	0.1	⋯	⋯	5.94	K2III	3	LPV
⋯	179522	110.02770	6e00	10.0	0.1	63153	⋯	7.42	G8III/IV	1	LPV
⋯	192594	32.91187	6e-02	35.0	0.6	⋯	⋯	7.35	K3 III	2	LPV
⋯	198752	73.25503	1e00	11.0	0.2	63815	⋯	7.13	K4III	2	LPV

Note. LPV: long period. ROT: rotation period. SPB: slowly pulsating B star.
References. (1) Houk (1978), (2) Houk (1982), (3) Houk & Cowley (1975), (4) Torres et al. (2006).

Table 9
Irregular Variables Detected with bRing

HD	VSX ID	P_{VSX} (day)	V (mag)	SpT	References
3359	⋯	⋯	8.39	K0V	1
4229	⋯	⋯	6.8	K5III	2
12440	⋯	⋯	8.19	K2III	2
36597	⋯	⋯	3.86	K1II/III	3
51801	55670	224.71910	7.15	K2/K3III	2
68809	⋯	⋯	7.93	K0III	1
69256	⋯	⋯	8.17	K0III	1
72838	⋯	⋯	7.25	K1Ib:	3
91869	⋯	⋯	6.9	G8/K0III+..	2
92063	43533	⋯	5.08	K1III	2
127755	58566	⋯	7.66	K3 III	2
128679	⋯	⋯	7.76	K2 III	2
139534	36907	295.39108	7.8	K0II/III	2
155806	33891	3.20848[a]	5.61	O8Ve	4
156468	33894	⋯	7.87	B2V:ne	3
158864	3633	⋯	8.17	B2 IB/IIeP	1
205834	⋯	⋯	8.1	K0 III	2
222060	⋯	⋯	5.99	K0II/III	2

Note.
[a] Rimoldini et al. (2012).
References. (1) Houk (1978), (2) Houk & Cowley (1975), (3) Houk (1982), (4) Sota et al. (2014).

(Luckas 2018; Rabus & Prieto 2018) or a young stellar object that underwent a burst of accretion (Strader et al. 2018). Given the proximity of the nova compared to the bRing pixel size, the light curve of HD 92063 is likely corrupted by ASASSN-18fv.

bRing also observed a few isolated dimming events in the stars HD 4229, HD 12440, HD 35324, and HD 222060; however, the events could not be verified as real, significant events due to their short duration and noisy characteristics. We also identified HD 36597, HD 51801, HD 139534, and HD 159468 as semi-regular variables in the bRing data.

HD 155806 (V1075 Sco) and HD 158864 (V830 Ara): V1075 Sco (O8V star classified as a Be in VSX) shows significant variability (amplitude of 0.05 mag) over the first 100 days of bRing data. After disappearing from the bRing data for about 100 more days, the star reappears as roughly constant. This is likely just a symptom of the irregularity exhibited by these stars. Since HD 155806 is not listed as a GCAS in any source, bRing simply classified this as an irregular star. V830 Ara showed several significant brightening events ($\simeq$0.2 mag) throughout the 500 days of observation. A representative period could not be converged on, so this was classified as irregular.

In Mamajek et al. (2012), the authors detected an unusually deep eclipsing event that took place over $\sim$50 days in the J1407 system; this light curve has been subsequently modeled as a circumplanetary ring system (van Werkhoven et al. 2014; Kenworthy & Mamajek 2015). Follow-up observations and a study of the archival photometry have attempted to deduce the periodic nature of this event, but an additional event has yet to be confirmed (Mentel et al. 2018). While searching for variables in the bRing data, evidence of such eclipses in other stars were also searched for. Unfortunately, no other eclipses of similar length or depth were detected.

5. Conclusion

The bRing survey of β Pictoris included nearly continuous photometric monitoring of 10,000+ bright variables in the southern sky (Stuik et al. 2017; Mellon et al. 2019b, 2019a). This paper reports on the variability of the bright ($V \simeq 4$–8 mag) stars observed during the bRing survey, and provides improved periods (and sometimes classifications) for many known variables, identifies new variables missed by previous surveys, and provides classifications for some VSX candidate variables. The light curves were also examined for any evidence of transits by circumstellar or circumplanetary dust disks or ring systems analogous to J1407 (V1400 Cen), but no such cases were observed.

Of the 16,762 analyzed in this survey, 353 stars were detected as variable (80% were previously known and 20% were new detections or classifications). These stars were separated by variability into several tables where identifying information and the bRing periods and amplitudes were provided. We provided a brief discussion on the stars whose periods or classifications deviated from those established by the VSX catalog or other surveys. We also provided brief discussion on the newly detected variables and the stars that should be reclassified to better fit their period, light-curve shape, and spectral type. bRing was able to measure the O'Connell effect in 18 of the contact binaries in this survey; only 2 of these had previously shown the asymmetry in their light curves. This survey also detected 18 irregular variables, which were briefly discussed. The results from this survey of the bRing time-series photometry provides initial assessments of the variability parameters for bright southern stars, and may provide opportunities for further study to constrain the nature of these new and reclassified variable stars.

S.N.M. is a U.S. Department of Defense SMART scholar sponsored by the U.S. Navy through NIWC-Atlantic. The results reported herein benefitted from collaborations and/or information exchange within NASA's Nexus for Exoplanet System Science (NExSS) research coordination network sponsored by NASA's Science Mission Directorate. Part of this research was carried out at the Jet Propulsion Laboratory, California Institute of Technology, under a contract with NASA. The authors would like to acknowledge the support staff at both the South African Astronomical Observatory and Siding Spring Observatory for keeping both bRing stations maintained and running. Construction of the bRing observatory to be sited at Siding Springs, Australia would not be possible without a University of Rochester University Research Award, help from Mike Culver and Rich Sarkis (UR), and generous donations of time, services, and materials from Joe and Debbie Bonvissuto of Freight Expediters, Michael Akkaoui and his team at Tanury Industries, Robert Harris and Michael Fay at BCI, Koch Division, Mark Paup, Dave Mellon, and Ray Miller and the Zippo Tool Room. This research has made use of the International Variable Star Index (VSX) database, operated at AAVSO, Cambridge, Massachusetts, USA. This research has made use of the VizieR catalog access tool, CDS, Strasbourg, France (doi:10.26093/cds/vizier). This research has made use of the SIMBAD database, operated at CDS, Strasbourg, France. We acknowledge with thanks the variable star observations from the AAVSO International Database contributed by observers worldwide and used in this research.

Facilities: bRing-SA, bRing-AU, AAVSO.

Software: Python 3.7.3 (Rossum 1995), scipy (Jones et al. 2001), matplotlib (Hunter 2007), numpy (Stéfan van der Walt & Varoquaux 2011), astropy (The Astropy Collaboration et al. 2018).

Appendix

Table 10 in the Appendix contains the adopted and calculated stellar parameters used to generate the color–magnitude diagram in Figure 4.

Table 10
Adopted and Calculated Stellar Parameters

Name …	l (deg)	b (deg)	ϖ (mas)	B (mag)	V (mag)	$(B-V)$ (mag)	$E(B-V)$ (mag)	$(B-V)_0$ (mag)	A_V (mag)	M_V (mag)
HD 3112	305.008486	−45.789165	7.162	6.359	6.109	0.250	0.005	0.245	0.015	0.369
HD 3359	309.594473	−67.800879	23.039	9.150	8.370	0.780	0.001	0.779	0.003	5.179
HD 3463	304.865029	−47.640183	5.377	8.240	8.040	0.200	0.008	0.192	0.025	1.668
HD 4229	303.190503	−31.421460	7.005	8.099	6.808	1.291	0.008	1.283	0.026	1.009
HD 4737	304.207519	−70.424430	7.996	7.175	6.277	0.898	0.002	0.896	0.006	0.785
HD 5135	302.466765	−65.577096	5.346	8.570	7.880	0.690	0.004	0.686	0.013	1.508
HD 6269	256.206003	−86.456746	7.841	7.213	6.283	0.930	0.002	0.928	0.006	0.749
HD 6882	297.833132	−61.714404	10.920	3.908	4.014	−0.106	0.002	−0.108	0.006	−0.801
HD 74422	278.644521	−12.886437	3.120	8.390	8.120	0.270	0.087	0.183	0.268	0.323
HD 8351	271.660105	−78.144661	7.234	6.960	6.698	0.262	0.002	0.260	0.006	0.989
HD 11413	280.699247	−64.277086	12.726	6.080	5.929	0.151	0.001	0.150	0.003	1.449
HD 11597	239.679217	−75.489274	12.648	8.610	8.150	0.460	0.001	0.459	0.003	3.657
HD 12284	246.808665	−73.257393	4.900	9.448	9.108	0.340	0.004	0.336	0.012	2.547
HD 12440	296.850833	−42.225420	2.537	9.500	8.200	1.300	0.030	1.270	0.098	0.124
HD 13397	272.939621	−63.724270	3.755	8.770	7.740	1.030	0.008	1.022	0.026	0.588
HD 16589	245.541212	−65.100855	17.948	6.995	6.483	0.512	0.001	0.511	0.003	2.750
HD 17084	244.720178	−64.175500	24.310	8.770	8.055	0.715	0.000	0.715	0.000	4.984
HD 17653	290.780175	−43.096853	17.029	7.120	6.660	0.460	0.002	0.458	0.006	2.810
HD 17755	283.036786	−49.418163	10.366	8.480	8.060	0.420	0.002	0.418	0.006	3.132
HD 20232	243.589022	−58.176492	12.584	7.040	6.880	0.160	0.001	0.159	0.003	2.376
HIP 21213	241.248424	−42.783693	7.500	7.800	7.630	0.170	0.001	0.169	0.003	2.002
HD 21765	276.560889	−47.102603	9.443	8.351	7.890	0.461	0.002	0.459	0.006	2.759
HD 25860	255.319180	−47.497443	7.153	6.826	6.615	0.211	0.002	0.209	0.006	0.881
HD 28837	245.182260	−43.294769	6.527	7.400	7.010	0.390	0.002	0.388	0.006	1.077

Table 10
(Continued)

Name	l (deg)	b (deg)	ϖ (mas)	B (mag)	V (mag)	$(B-V)$ (mag)	$E(B-V)$ (mag)	$(B-V)_0$ (mag)	A_V (mag)	M_V (mag)
HD 30551	255.898732	−40.347787	0.870	8.990	6.350	2.640	0.012	2.628	0.042	−3.995
HD 30861	253.109163	−39.985308	4.691	7.580	7.440	0.140	0.003	0.137	0.009	0.787
HD 31407	264.090685	−38.718807	0.967	7.470	7.690	−0.220	0.013	−0.233	0.039	−2.422
HD 32453	243.737596	−37.381308	8.017	6.918	6.007	0.911	0.001	0.910	0.003	0.524
HD 32846	238.873189	−36.257079	10.170	6.607	6.314	0.293	0.001	0.292	0.003	1.348
HD 33331	250.226912	−36.738948	3.390	6.806	6.892	−0.086	0.005	−0.091	0.015	−0.472
HD 34349	275.285824	−34.809895	16.128	7.450	7.050	0.400	0.001	0.399	0.003	3.085
HD 34802	289.295356	−31.915956	5.409	8.850	7.770	1.080	0.030	1.050	0.097	1.339
HD 35324	282.662535	−33.019396	4.625	9.060	7.720	1.340	0.023	1.317	0.075	0.971
HIP 35815	251.367772	−11.077202	4.515	8.200	7.840	0.360	0.008	0.352	0.025	1.088
HD 36597	239.889723	−30.875387	12.461	5.010	3.870	1.140	0.001	1.139	0.003	−0.655
HD 36705	275.300830	−33.045550	65.320	7.856	6.999	0.857	0.000	0.857	0.000	6.074
HD 37350	271.733779	−32.774457	3.112	4.580	3.760	0.820	0.014	0.806	0.045	−3.819
HD 37513	287.845391	−31.095793	9.644	8.800	8.240	0.560	0.003	0.557	0.009	3.152
HD 37909	293.876606	−29.872461	6.892	8.510	8.260	0.250	0.008	0.242	0.025	2.427
HD 39244	252.963719	−29.692239	6.456	7.770	7.530	0.240	0.002	0.238	0.006	1.574
HD 39764	239.361225	−26.094313	9.666	4.720	4.870	−0.150	0.001	−0.151	0.003	−0.207
HD 39917	250.029969	−28.401647	5.307	8.660	7.906	0.754	0.003	0.751	0.010	1.521
HD 39937	265.481354	−30.410684	8.536	6.582	5.948	0.634	0.001	0.633	0.003	0.601
HD 41846	280.357024	−29.637540	5.192	8.470	8.110	0.360	0.014	0.346	0.044	1.643
HD 42504	262.654416	−27.941484	2.656	8.690	7.700	0.990	0.022	0.968	0.071	−0.250
HD 42933	263.302876	−27.683668	2.510	4.580	4.810	−0.230	0.027	−0.257	0.081	−3.273
HD 43518	268.921715	−27.999235	3.870	8.700	7.410	1.290	0.009	1.281	0.029	0.319
HD 43898	243.230633	−22.045071	6.925	8.160	7.870	0.290	0.002	0.288	0.006	2.066
HD 46291	282.691975	−27.681412	3.468	9.370	8.261	1.109	0.040	1.069	0.129	0.832
HD 46586	256.476067	−22.936854	8.882	8.320	8.030	0.290	0.001	0.289	0.003	2.770
HD 46697	268.279215	−25.562813	6.924	8.790	7.739	1.051	0.003	1.048	0.010	1.931
HD 46978	295.054679	−27.916876	5.090	8.480	8.160	0.320	0.073	0.247	0.226	1.468
HD 49877	265.125175	−22.645861	4.812	7.190	5.610	1.580	0.007	1.573	0.023	−1.001
HD 51801	281.264333	−25.361915	2.414	8.510	7.140	1.370	0.049	1.321	0.160	−1.107
HD 52993	246.244795	−13.439255	4.336	6.416	6.569	−0.153	0.007	−0.160	0.021	−0.267
HD 53143	271.654979	−22.592123	54.466	7.609	6.803	0.806	0.000	0.806	0.000	5.484
HD 54579	246.104700	−12.009698	15.469	8.940	8.029	0.911	0.001	0.910	0.003	3.973
HD 55173	242.507518	−9.724266	1.014	7.320	7.490	−0.170	0.049	−0.219	0.148	−2.628
HD 56142	248.137346	−11.516440	4.202	8.140	7.590	0.550	0.008	0.542	0.025	0.682
HD 56146	270.588989	−20.723588	2.261	8.050	8.090	−0.040	0.091	−0.131	0.276	−0.414
HD 56910	269.431682	−19.896621	6.452	7.100	6.840	0.260	0.005	0.255	0.015	0.873
HD 57969	267.448737	−18.489199	13.850	6.670	6.560	0.110	0.001	0.109	0.003	2.264
HD 58635	249.869298	−9.996722	5.520	7.100	6.810	0.290	0.006	0.284	0.019	0.501
HD 60168	249.247507	−8.119752	4.071	6.540	6.617	−0.077	0.010	−0.087	0.030	−0.365
HD 60559	253.130100	−9.785495	4.435	6.130	6.247	−0.117	0.011	−0.128	0.033	−0.552
HD 60649	265.536902	−15.781967	1.868	6.900	7.000	−0.100	0.109	−0.209	0.329	−1.972
HD 61330	248.978598	−6.669998	9.050	4.440	4.530	−0.090	0.002	−0.092	0.006	−0.693
HD 61644	273.717460	−18.682117	2.270	8.480	8.410	0.070	0.138	−0.068	0.419	−0.229
HD 63203	269.250591	−15.590387	1.914	8.300	8.320	−0.020	0.111	−0.131	0.336	−0.606
HD 63786	250.416015	−4.687935	6.539	5.886	5.936	−0.050	0.005	−0.055	0.015	−0.002
HD 64503	253.899409	−5.925270	5.030	4.301	4.474	−0.173	0.010	−0.183	0.030	−2.048
HD 64722	267.614913	−13.538668	2.313	5.529	5.680	−0.151	0.140	−0.291	0.420	−2.919
HD 65592	255.495365	−5.718947	0.802	8.130	7.370	0.760	0.356	0.404	1.110	−4.219
HD 65818	263.475590	−10.279223	3.400	4.240	4.410	−0.170	0.054	−0.224	0.163	−3.095
HD 66235	260.267567	−7.955540	2.508	7.540	7.670	−0.130	0.029	−0.159	0.088	−0.421
HD 66260	274.638128	−16.135648	5.388	7.760	7.460	0.300	0.016	0.284	0.050	1.068
HD 66503	258.189795	−6.404198	2.190	8.126	8.220	−0.094	0.025	−0.119	0.076	−0.154
HD 66623	251.745048	−2.180114	12.137	8.680	8.143	0.537	0.001	0.536	0.003	3.560
HD 66768	269.364185	−12.874937	2.557	6.660	6.690	−0.030	0.187	−0.217	0.564	−1.835
HD 68556	263.228698	−7.694949	0.616	8.780	8.160	0.620	0.120	0.500	0.376	−3.268
HD 68808	262.440856	−6.959550	1.217	6.350	5.760	0.590	0.066	0.524	0.207	−4.021
HD 68809	263.924453	−7.933014	2.491	9.070	7.930	1.140	0.042	1.098	0.136	−0.224
HD 68860	252.427475	−0.187155	0.584	8.000	6.700	1.300	0.202	1.098	0.653	−5.120
HD 69213	260.894205	−5.528365	9.858	6.980	6.700	0.280	0.002	0.278	0.006	1.663
HD 69256	262.640578	−6.653319	3.475	9.310	8.200	1.110	0.023	1.087	0.074	0.830
HD 69342	258.843122	−4.020185	…	8.240	8.060	0.180	…	…	…	…
HD 69879	249.199313	3.217249	7.055	7.475	6.422	1.053	0.004	1.049	0.013	0.652

Table 10
(Continued)

Name	l (deg)	b (deg)	ϖ (mas)	B (mag)	V (mag)	$(B-V)$ (mag)	$E(B-V)$ (mag)	$(B-V)_0$ (mag)	A_V (mag)	M_V (mag)
HD 69882	259.498710	−3.908606	0.525	7.480	7.170	0.310	0.280	0.030	0.855	−5.085
HD 70999	256.821157	−0.612875	1.472	7.930	8.050	−0.120	0.113	−0.233	0.340	−1.450
HD 71302	260.502870	−2.888402	1.820	5.900	6.020	−0.120	0.065	−0.185	0.196	−2.876
HD 71487	257.618591	−0.538006	5.820	6.660	6.500	0.160	0.009	0.151	0.028	0.297
HD 71801	254.604570	2.030543	1.626	5.600	5.740	−0.140	0.062	−0.202	0.187	−3.391
HD 72275	275.249545	−12.285240	0.760	8.140	7.310	0.830	0.150	0.680	0.474	−3.760
HD 72698	274.678126	−11.515123	2.634	8.130	8.060	0.070	0.103	−0.033	0.314	−0.151
HD 72754	266.826694	−5.815158	0.582	9.090	8.880	0.210	0.231	−0.021	0.704	−2.999
HD 72838	266.517046	−5.480196	0.613	9.020	7.270	1.750	0.216	1.534	0.714	−4.505
HD 72878	271.659765	−9.204825	1.900	7.520	7.460	0.060	0.110	−0.050	0.335	−1.481
HD 72979	284.687144	−17.945936	4.154	7.900	7.700	0.200	0.045	0.155	0.138	0.654
HD 73141	267.079253	−5.553821	1.925	8.310	8.410	−0.100	0.098	−0.198	0.296	−0.464
HD 73340	268.266544	−6.176067	6.705	5.651	5.782	−0.131	0.005	−0.136	0.015	−0.101
HD 73502	262.882000	−1.910762	0.547	8.507	7.260	1.247	0.186	1.061	0.600	−4.651
HD 73699	259.795991	0.695547	1.004	7.620	7.600	0.020	0.087	−0.067	0.264	−2.656
HD 73882	260.181611	0.643141	2.170	7.590	7.190	0.400	0.036	0.364	0.112	−1.240
HD 74195	270.250715	−6.800198	6.610	3.440	3.630	−0.190	0.005	−0.195	0.015	−2.284
HD 74531	266.684501	−3.612202	1.331	7.080	7.230	−0.150	0.100	−0.250	0.301	−2.450
HD 74712	266.194768	−3.002906	0.258	9.580	8.320	1.260	0.230	1.030	0.741	−5.361
HD 74884	265.493657	−2.179077	0.409	9.190	8.330	0.860	0.312	0.548	0.980	−4.593
HD 75747	292.550759	−21.631893	10.096	6.280	6.070	0.210	0.005	0.205	0.015	1.075
HD 76006	268.697008	−3.333926	0.677	8.880	8.550	0.330	0.155	0.175	0.477	−2.773
HD 76566	265.641514	0.054159	2.601	6.100	6.260	−0.160	0.025	−0.185	0.075	−1.739
HD 76640	275.750650	−8.474583	4.580	6.257	6.353	−0.096	0.029	−0.125	0.088	−0.431
HD 76875	269.870923	−3.179071	2.681	8.830	7.720	1.110	0.031	1.079	0.100	−0.238
HD 77347	273.102827	−5.381860	4.675	7.840	7.580	0.260	0.019	0.241	0.059	0.870
HD 77464	271.159400	−3.523334	1.534	6.550	6.690	−0.140	0.054	−0.194	0.163	−2.544
HD 77581	263.058292	3.929854	0.384	7.370	6.870	0.500	0.142	0.358	0.442	−5.651
HD 77653	271.749887	−3.811274	8.850	5.171	5.295	−0.124	0.003	−0.127	0.009	0.021
HD 77669	265.662442	0.121400	1.955	8.050	8.100	−0.050	0.040	−0.090	0.121	−0.565
HD 78165	264.674744	3.317533	2.912	7.820	7.610	0.210	0.021	0.189	0.065	−0.134
HD 78405	272.634839	−3.739767	1.764	8.150	8.260	−0.110	0.049	−0.159	0.148	−0.655
HD 78763	285.437818	−14.797121	1.902	8.270	8.310	−0.040	0.066	−0.106	0.200	−0.494
HD 78801	271.863164	−2.558817	1.007	8.820	7.690	1.130	0.076	1.054	0.245	−2.539
HD 79039	269.132131	0.321652	2.273	6.692	6.812	−0.120	0.029	−0.149	0.088	−1.493
HD 81222	276.569793	−4.194508	0.911	8.290	7.570	0.720	0.217	0.503	0.680	−3.312
HD 81654	278.728196	−5.905462	0.916	7.880	7.880	0.000	0.176	−0.176	0.532	−2.843
HD 81771	288.159479	−15.200061	3.475	7.970	7.760	0.210	0.086	0.124	0.264	0.201
HD 82484	266.475505	8.320205	2.664	8.300	8.090	0.210	0.039	0.171	0.120	0.098
HD 82829	270.382574	4.770436	5.973	8.050	7.810	0.240	0.012	0.228	0.037	1.654
HD 84400	275.668170	1.411384	2.413	6.061	6.168	−0.107	0.043	−0.150	0.130	−2.050
HD 84416	285.886712	−10.535299	6.407	6.390	6.320	0.070	0.014	0.056	0.043	0.310
HD 84810	283.199003	−7.003808	0.777	4.330	3.400	0.930	0.156	0.774	0.496	−7.643
HD 85037	275.356375	2.830386	7.345	6.660	6.530	0.130	0.008	0.122	0.025	0.835
HD 85185	274.208898	4.519312	2.817	8.040	8.010	0.030	0.032	−0.002	0.098	0.161
HD 85871	279.410387	−0.870275	1.185	8.900	6.491	2.409	0.091	2.318	0.313	−3.453
HD 85953	276.869760	2.510135	1.684	5.777	5.932	−0.155	0.056	−0.211	0.169	−3.105
HD 86118	281.478387	−3.120892	1.341	6.470	6.640	−0.170	0.100	−0.270	0.301	−3.024
HD 86441	281.231910	−2.339378	1.033	7.490	7.520	−0.030	0.163	−0.193	0.492	−2.901
HD 87072	286.854973	−8.911832	0.858	9.070	8.290	0.780	0.155	0.625	0.489	−2.532
HD 87896	285.865065	−6.593891	6.670	7.820	6.910	0.910	0.015	0.895	0.048	0.983
HD 88278	295.294369	−18.743258	4.663	7.550	7.310	0.240	0.175	0.065	0.536	0.118
HD 88824	279.384303	4.265916	20.186	5.519	5.265	0.254	0.003	0.251	0.009	1.781
HD 88825	284.272213	−2.915781	1.455	5.997	6.087	−0.090	0.077	−0.167	0.233	−3.331
HD 89611	277.070166	9.457440	2.421	7.980	7.960	0.020	0.021	−0.001	0.064	−0.184
HD 89841	282.568898	1.474929	0.610	9.710	7.860	1.850	0.177	1.673	0.589	−3.803
HD 90000	279.472330	6.656732	1.299	7.420	7.560	−0.140	0.070	−0.210	0.211	−2.084
HD 90611	279.233514	8.442773	9.683	6.830	6.550	0.280	0.004	0.276	0.012	1.468
HD 90885	282.046388	4.407698	29.660	9.140	8.331	0.809	0.001	0.808	0.003	5.689
HD 90941	280.261842	7.510635	1.770	8.400	7.810	0.590	0.061	0.529	0.191	−1.142
HD 91519	273.992190	18.937293	4.197	7.980	7.700	0.280	0.030	0.250	0.093	0.722
HD 91869	285.492104	0.502151	2.070	7.790	6.910	0.880	0.046	0.834	0.147	−1.657
HD 92063	286.572675	−1.053904	13.237	6.249	5.088	1.161	0.010	1.151	0.032	0.664

Table 10
(Continued)

Name	l	b	ϖ	B	V	$(B-V)$	$E(B-V)$	$(B-V)_0$	A_V	M_V
...	(deg)	(deg)	(mas)	(mag)	(mag)	(mag)	(mag)	(mag)	(mag)	(mag)
HD 92287	285.630996	1.065114	2.666	5.749	5.876	−0.127	0.038	−0.165	0.115	−2.109
HD 92762	296.898420	−18.231703	7.730	8.060	7.810	0.250	0.009	0.241	0.028	2.223
HD 93130	287.568572	−0.859319	0.359	8.310	8.040	0.270	0.397	−0.127	1.202	−5.389
HD 93203	286.547631	1.212855	0.512	7.700	6.870	0.830	0.230	0.600	0.724	−5.308
HD 93486	298.409551	−20.324017	5.724	8.540	8.090	0.450	0.034	0.416	0.106	1.773
HD 93668	284.507820	6.151308	4.593	6.730	6.740	−0.010	0.020	−0.030	0.061	−0.010
HD 94924	292.748165	−8.238385	4.349	8.130	8.010	0.120	0.122	−0.002	0.372	0.830
HD 94985	285.137134	8.114793	9.124	6.061	5.898	0.163	0.006	0.157	0.018	0.680
HD 95109	289.057053	0.042811	0.479	7.210	6.110	1.100	0.400	0.700	1.267	−6.755
HD 95752	291.393564	−3.915900	0.314	7.421	6.970	0.451	0.447	0.004	1.364	−6.909
HD 95993	291.028404	−2.723612	2.260	8.620	8.180	0.440	0.245	0.195	0.755	−0.804
HD 97082	290.085281	1.472661	0.796	7.590	6.790	0.800	0.164	0.636	0.518	−4.224
HD 97152	290.946906	−0.488398	0.371	8.030	8.070	−0.040	0.352	−0.392	1.051	−5.133
HD 97485	291.472695	−1.111831	0.704	8.830	7.900	0.930	0.236	0.694	0.747	−3.610
HD 99757	289.751623	9.870446	2.160	8.060	8.160	−0.100	0.036	−0.136	0.109	−0.277
HD 100148	292.067042	4.264463	0.326	8.900	8.190	0.710	0.208	0.502	0.652	−4.894
HD 100213	294.807873	−4.144356	0.422	9.520	9.340	0.180	0.499	−0.319	1.495	−4.027
HD 100359	297.394601	−11.893218	1.867	7.081	6.884	0.197	0.323	−0.126	0.978	−2.739
HD 101947	295.179035	−0.644405	0.588	5.830	5.030	0.800	0.253	0.547	0.795	−6.917
HD 102541	290.030770	20.985574	8.604	8.180	7.940	0.240	0.006	0.234	0.019	2.595
HD 102682	291.846064	15.305595	3.918	8.789	8.240	0.549	0.052	0.497	0.163	1.042
HD 102893	295.568451	1.204261	1.120	8.280	8.250	0.030	0.147	−0.117	0.445	−1.949
HD 103285	296.026562	0.811795	1.347	8.310	8.240	0.070	0.138	−0.068	0.419	−1.533
HD 104036	300.068148	−15.248520	9.566	6.918	6.738	0.180	0.009	0.171	0.028	1.614
HD 104631	297.305591	0.165498	0.464	6.808	6.771	0.037	0.372	−0.335	1.114	−6.010
HD 104705	297.454691	−0.336299	0.432	9.560	9.110	0.450	0.386	0.064	1.181	−3.891
HD 105509	294.957397	17.886055	10.916	5.991	5.746	0.245	0.006	0.239	0.019	0.918
HD 106111	299.636182	−7.527775	1.131	7.010	6.170	0.840	0.227	0.613	0.716	−4.277
HIP 107231	349.866388	−48.057946	4.028	8.530	8.260	0.270	0.010	0.260	0.031	1.255
HD 107805	299.633990	1.064419	1.980	7.000	6.420	0.580	0.149	0.431	0.465	−2.562
HD 108015	298.254125	15.478414	0.212	8.379	7.960	0.419	0.064	0.355	0.199	−5.605
HD 108968	300.416306	3.351249	1.778	6.190	5.530	0.660	0.153	0.507	0.480	−3.700
HD 110080	302.015990	−7.694393	5.956	7.670	7.410	0.260	0.071	0.189	0.219	1.066
HD 110258	301.672146	3.053100	0.621	9.050	8.265	0.785	0.253	0.532	0.794	−3.564
HD 110311	302.104209	−6.550839	1.000	7.110	6.330	0.780	0.191	0.589	0.601	−4.271
HD 111984	303.343188	19.794944	6.910	7.510	7.280	0.230	0.028	0.202	0.086	1.391
HD 112044	303.316382	4.438949	1.022	7.340	6.580	0.760	0.218	0.542	0.685	−4.058
HD 112999	304.174646	2.175884	1.338	7.414	7.383	0.031	0.289	−0.258	0.869	−2.853
HD 114529	305.545614	2.845291	8.610	4.500	4.593	−0.093	0.019	−0.112	0.058	−0.790
HD 115823	307.408458	9.870003	8.166	5.314	5.443	−0.129	0.014	−0.143	0.042	−0.039
HD 116862	308.917726	13.072689	1.255	6.126	6.257	−0.131	0.075	−0.206	0.226	−3.476
HD 117399	307.686744	0.918454	0.484	7.190	6.490	0.700	0.451	0.249	1.394	−6.481
HD 118258	309.271499	6.154131	9.360	8.840	8.040	0.800	0.014	0.786	0.045	2.852
HD 118769	309.462365	4.637572	0.537	8.720	7.300	1.420	0.225	1.195	0.731	−4.780
HD 119888	309.107132	−1.669995	0.540	7.880	7.880	0.000	0.308	−0.308	0.924	−4.382
HD 120400	310.839533	4.377956	0.841	8.440	7.690	0.750	0.161	0.589	0.507	−3.192
HD 121191	312.441366	8.159707	7.570	8.400	8.160	0.240	0.020	0.220	0.062	2.494
HD 121291	314.795173	16.737341	0.996	8.640	7.900	0.740	0.054	0.686	0.171	−2.279
HD 122314	309.986969	−4.857728	6.034	7.970	7.620	0.350	0.063	0.287	0.195	1.328
HD 122844	313.625108	6.651686	7.752	6.433	6.204	0.229	0.026	0.203	0.080	0.571
HD 123720	314.119582	5.685342	6.262	7.980	7.750	0.230	0.044	0.186	0.136	1.598
HD 124195	314.733924	6.351017	3.726	6.130	6.090	0.040	0.185	−0.145	0.560	−1.614
HD 124672	310.895742	−6.521600	15.482	8.070	7.550	0.520	0.008	0.512	0.025	3.474
HD 124689	314.132939	3.145630	9.267	7.650	7.290	0.360	0.020	0.340	0.062	2.063
HD 125104	315.068011	4.908926	1.529	7.360	7.300	0.060	0.266	−0.206	0.802	−2.580
HD 125721	318.197805	11.829894	1.047	8.840	8.490	0.350	0.114	0.236	0.352	−1.762
HD 125823	321.565642	20.022614	7.130	4.240	4.420	−0.180	0.013	−0.193	0.039	−1.354
HD 126859	316.399573	4.142315	7.032	7.189	6.965	0.224	0.063	0.161	0.194	1.006
HD 127297	316.444594	3.307587	1.340	7.840	6.930	0.910	0.284	0.626	0.896	−3.331
HD 127755	315.349490	−0.303711	0.710	9.430	7.630	1.800	0.340	1.460	1.120	−4.233
HD 127972	322.773998	16.669138	10.670	2.120	2.310	−0.190	0.009	−0.199	0.027	−2.576
HD 128679	308.950206	−16.205993	2.853	9.090	7.760	1.330	0.077	1.253	0.251	−0.214
HD 129094	314.416788	−4.710796	9.186	9.920	9.460	0.460	0.000	0.460	0.000	4.276

Table 10
(Continued)

Name …	l (deg)	b (deg)	ϖ (mas)	B (mag)	V (mag)	$(B-V)$ (mag)	$E(B-V)$ (mag)	$(B-V)_0$ (mag)	A_V (mag)	M_V (mag)
HD 129118	323.658227	15.582768	6.354	7.780	6.790	0.990	0.014	0.976	0.045	0.760
HD 130233	313.973805	−7.214961	1.016	8.290	7.440	0.850	0.180	0.670	0.569	−3.095
HD 130701	315.825304	−4.013205	1.745	6.660	5.960	0.700	0.133	0.567	0.418	−3.249
HD 131638	325.032748	12.542091	2.462	8.330	8.320	0.010	0.062	−0.052	0.189	0.088
HD 132247	323.127179	7.800860	4.932	8.270	8.090	0.180	0.052	0.128	0.160	1.396
HD 133880	329.181429	15.214997	9.652	5.650	5.790	−0.140	0.011	−0.151	0.033	0.680
HD 135240	319.688221	−2.911210	1.556	5.030	5.090	−0.060	0.152	−0.212	0.458	−4.408
HD 135411	332.251211	16.998319	1.070	9.900	8.220	1.680	0.097	1.583	0.321	−1.954
HD 135592	316.976839	−7.757915	1.475	6.960	6.390	0.570	0.116	0.454	0.363	−3.128
HD 135876	330.846349	13.954524	6.974	5.495	5.604	−0.109	0.012	−0.121	0.036	−0.215
HD 136633	319.961709	−4.261537	1.143	8.280	8.230	0.050	0.171	−0.121	0.518	−1.998
HD 137164	319.624925	−5.332615	8.763	9.180	8.140	1.040	0.019	1.021	0.061	2.792
HD 137518	329.807083	9.395976	0.582	7.830	7.750	0.080	0.178	−0.098	0.540	−3.964
HD 137626	318.422350	−7.641804	0.889	8.610	7.800	0.810	0.141	0.669	0.446	−2.902
HD 138521	317.798582	−9.522212	3.742	8.050	8.040	0.010	0.062	−0.052	0.189	0.717
HD 139534	319.148827	−8.694991	4.067	8.810	7.810	1.000	0.065	0.935	0.208	0.648
HD 140566	332.392135	7.543717	3.791	8.510	8.290	0.220	0.064	0.156	0.197	0.987
HD 142049	323.988673	0.015545	19.510	6.210	5.850	0.360	0.005	0.355	0.016	2.286
HD 142542	342.704106	16.465330	18.766	6.718	6.284	0.434	0.003	0.431	0.009	2.642
HD 142941	322.129487	−8.223853	1.075	7.190	6.410	0.780	0.092	0.688	0.291	−3.724
HD 142994	338.396060	10.867654	6.347	7.460	7.170	0.290	0.011	0.279	0.034	1.149
HD 143028	321.769239	−8.741536	0.706	7.720	7.800	−0.080	0.105	−0.185	0.317	−3.273
HD 143098	340.463665	12.953532	30.331	8.330	7.640	0.690	0.002	0.688	0.006	5.043
HD 143232	338.403332	10.406861	6.784	6.890	6.660	0.230	0.008	0.222	0.025	0.793
HD 143999	323.231855	−8.042597	0.877	8.430	7.890	0.540	0.111	0.429	0.346	−2.741
HD 144951	328.159706	−3.508135	0.940	8.080	8.070	0.010	0.251	−0.241	0.755	−2.821
HD 146323	327.753558	−5.403478	1.062	7.490	6.490	1.000	0.192	0.808	0.611	−3.992
HD 147170	333.339110	−0.575511	4.619	8.895	8.263	0.632	0.101	0.531	0.317	1.269
HD 147683	344.856604	10.088824	3.387	7.160	7.050	0.110	0.355	−0.245	1.068	−1.369
HD 147894	335.606579	0.682539	6.090	7.241	7.312	−0.071	0.081	−0.152	0.245	0.990
HD 148891	315.735663	−18.647736	3.946	8.050	8.000	0.050	0.044	0.006	0.134	0.846
HD 149238	324.027972	−11.927103	18.618	8.580	8.040	0.540	0.006	0.534	0.019	4.371
HD 149404	340.537543	3.005780	0.760	5.880	5.520	0.360	0.442	−0.082	1.342	−6.419
HD 149450	338.788613	1.271181	1.121	8.229	8.239	−0.010	0.262	−0.272	0.787	−2.300
HD 149455	331.781126	−5.212324	4.271	7.710	7.690	0.020	0.149	−0.129	0.451	0.391
HD 149668	327.191739	−9.577443	2.115	7.710	7.610	0.100	0.079	0.021	0.241	−1.004
HD 149715	330.389958	−6.781829	3.569	9.420	8.330	1.090	0.135	0.955	0.433	0.659
HD 149779	339.877907	1.797286	1.154	7.740	7.560	0.180	0.306	−0.126	0.927	−3.056
HD 151158	341.876698	1.450784	0.856	8.480	8.250	0.230	0.419	−0.189	1.265	−3.353
HD 151475	338.875985	−1.588860	0.992	8.170	8.060	0.110	0.266	−0.156	0.804	−2.762
HD 151564	343.130554	1.910493	0.737	8.100	7.980	0.120	0.438	−0.318	1.313	−3.995
HD 151665	315.626975	−20.092090	2.907	8.320	8.070	0.250	0.056	0.194	0.173	0.215
HD 151890	346.115149	3.913990	3.726	2.820	2.980	−0.160	0.181	−0.341	0.542	−4.705
HD 152333	343.827246	1.374939	0.735	8.930	8.840	0.090	0.434	−0.344	1.299	−3.128
HD 152478	336.782978	−4.635986	3.222	6.310	6.330	−0.020	0.244	−0.264	0.733	−1.863
HD 152511	328.996568	−10.888160	4.900	6.468	6.530	−0.062	0.058	−0.120	0.176	−0.195
HD 152667	344.531027	1.457096	0.607	6.510	6.220	0.290	0.436	−0.146	1.319	−6.183
HD 152901	346.897945	3.025074	3.115	7.450	7.390	0.060	0.187	−0.127	0.566	−0.709
HD 153004	350.412633	5.666730	2.270	7.370	6.610	0.760	0.272	0.488	0.852	−2.462
HD 153140	340.596082	−2.424087	0.926	7.850	7.500	0.350	0.327	0.023	0.999	−3.665
HD 153747	347.139655	1.962184	5.469	7.540	7.420	0.120	0.033	0.087	0.101	1.008
HD 153919	347.754424	2.173487	0.549	6.780	6.510	0.270	0.402	−0.132	1.217	−6.011
HD 154339	340.795488	−3.813101	0.837	9.740	9.190	0.550	0.345	0.205	1.064	−2.259
HD 155190	328.390770	−13.744251	4.083	7.100	7.130	−0.030	0.060	−0.090	0.182	0.003
HD 155550	352.960668	3.540731	0.641	8.130	8.070	0.060	0.328	−0.268	0.986	−3.881
HD 155555	324.898586	−16.297357	32.780	7.499	6.723	0.776	0.003	0.773	0.010	4.292
HD 155775	348.796715	0.145558	0.877	8.660	8.610	0.050	0.306	−0.256	0.920	−2.595
HD 155781	330.235394	0.180648	3.986	7.550	7.420	0.130	0.059	0.071	0.181	0.242
HD 156408	349.316308	−0.389699	3.378	8.650	8.270	0.380	0.192	0.188	0.592	0.322
HD 156623	343.479370	−4.832280	8.948	7.350	7.260	0.090	0.008	0.082	0.025	1.994
HD 156768	333.053617	−12.071444	2.980	7.016	5.872	1.144	0.079	1.065	0.255	−2.012
HD 156853	340.014519	−7.486891	2.747	7.560	7.600	−0.040	0.116	−0.156	0.351	−0.557
HD 156979	343.510397	−5.220728	0.977	7.670	6.740	0.930	0.245	0.685	0.775	−4.086

Table 10
(Continued)

Name	l (deg)	b (deg)	ϖ (mas)	B (mag)	V (mag)	$(B-V)$ (mag)	$E(B-V)$ (mag)	$(B-V)_0$ (mag)	A_V (mag)	M_V (mag)
HD 157321	327.178343	−16.158987	3.939	8.350	8.020	0.330	0.051	0.279	0.158	0.839
HD 158155	354.660584	0.814982	0.712	8.720	8.330	0.390	0.389	0.001	1.187	−3.594
HD 158186	355.906751	1.596463	0.940	7.070	7.040	0.030	0.268	−0.238	0.807	−3.902
HD 158443	354.359038	0.173160	0.920	8.780	7.910	0.870	0.298	0.572	0.937	−3.207
HD 159041	342.732780	−8.188957	1.634	7.990	8.040	−0.050	0.079	−0.129	0.239	−1.133
HD 159441	335.178910	−13.204213	9.550	7.690	7.360	0.330	0.008	0.322	0.025	2.235
HD 159654	349.029646	−4.865982	0.840	7.990	7.260	0.730	0.199	0.531	0.625	−3.744
HD 160589	356.568493	−1.268251	5.326	8.180	7.850	0.330	0.051	0.279	0.158	1.324
HD 161592	1.166282	0.209286	3.431	5.340	4.540	0.800	0.173	0.627	0.546	−3.328
HD 161783	338.940199	−13.195838	1.973	5.600	5.710	−0.110	0.122	−0.232	0.367	−3.182
HD 162102	356.489248	−3.419668	0.798	8.790	7.510	1.280	0.280	1.000	0.901	−3.882
HD 163181	358.125130	−3.774663	0.511	6.990	6.610	0.380	0.372	0.008	1.135	−5.984
HD 163254	349.894016	−8.614876	1.730	6.632	6.728	−0.096	0.083	−0.179	0.251	−2.333
HD 163482	355.219541	−5.828797	7.071	6.870	6.830	0.040	0.024	0.016	0.073	1.004
HD 163708	354.530336	−6.509347	5.712	7.155	7.089	0.066	0.033	0.033	0.101	0.772
HD 164975	1.575794	−3.979580	1.180	5.470	4.690	0.780	0.119	0.661	0.376	−5.327
HD 166596	351.887336	−10.965792	1.643	5.298	5.462	−0.164	0.053	−0.217	0.160	−3.619
HD 167231	357.282255	−8.844732	3.292	7.520	7.420	0.100	0.050	0.050	0.153	−0.145
HD 167714	313.739664	−25.774726	9.226	7.133	5.946	1.187	0.007	1.180	0.023	0.748
HD 168403	354.693942	−11.317882	4.582	6.900	6.790	0.110	0.027	0.083	0.083	0.012
HD 168651	346.130512	−15.563721	9.614	7.700	7.400	0.300	0.008	0.292	0.025	2.290
HD 168740	331.834147	−21.150130	14.147	6.313	6.122	0.191	0.006	0.185	0.018	1.857
HD 170461	357.594735	−12.142131	10.493	7.280	6.980	0.300	0.006	0.294	0.019	2.066
HD 171577	352.316173	−15.758740	3.472	7.780	7.750	0.030	0.037	−0.007	0.113	0.340
HD 171819	347.618520	−17.856894	10.163	6.058	5.840	0.218	0.008	0.210	0.025	0.850
HD 172416	347.960987	−18.296431	12.444	7.080	6.620	0.460	0.007	0.453	0.022	2.073
HD 172995	347.659912	−18.979164	6.290	7.010	6.810	0.200	0.018	0.182	0.055	0.748
HD 173344	332.368984	−23.771926	6.866	7.590	7.410	0.180	0.014	0.166	0.043	1.551
HD 173794	344.012056	−20.878022	6.220	7.350	7.120	0.230	0.020	0.210	0.062	1.027
HD 174139	338.884357	−22.668354	3.165	8.240	8.170	0.070	0.047	0.023	0.144	0.528
HD 174632	5.157964	−13.722970	4.227	6.607	6.638	−0.031	0.056	−0.087	0.170	−0.402
HD 174694	328.286503	−25.387694	5.199	5.080	4.400	0.680	0.016	0.664	0.051	−2.071
HD 175008	323.165007	−26.345258	5.397	6.750	6.790	−0.040	0.011	−0.051	0.033	0.417
HD 177171	344.540829	−23.346929	16.990	5.700	5.174	0.526	0.006	0.520	0.019	1.306
HD 177523	349.613583	−22.216656	7.289	7.780	7.490	0.290	0.012	0.278	0.037	1.766
HD 177665	351.911604	−21.656600	5.185	8.690	8.360	0.330	0.025	0.305	0.078	1.856
HD 177776	340.946298	−24.572862	3.143	8.150	8.120	0.030	0.038	−0.008	0.116	0.491
HD 179522	349.644068	−23.582311	8.066	8.330	7.430	0.900	0.010	0.890	0.032	1.931
HD 184035	358.915878	−24.806037	6.696	6.000	5.910	0.090	0.019	0.071	0.058	−0.019
HD 185139	353.528055	−27.057738	9.902	6.530	6.260	0.270	0.007	0.263	0.022	1.217
HD 187418	352.217174	−29.447853	3.583	8.590	8.310	0.280	0.019	0.261	0.059	1.023
HD 189631	358.788751	−30.384035	11.087	7.840	7.540	0.300	0.006	0.294	0.019	2.746
HD 189951	354.800696	−31.301714	5.250	8.100	7.830	0.270	0.012	0.258	0.037	1.394
HD 191585	331.765945	−33.205593	5.120	7.060	6.920	0.140	0.014	0.126	0.043	0.423
HD 192316	314.682531	−30.934019	7.588	7.770	7.550	0.220	0.007	0.213	0.022	1.929
HD 192594	2.167096	−32.659315	3.073	8.700	7.340	1.360	0.025	1.335	0.082	−0.304
HD 193174	9.694296	−31.884618	7.106	7.500	7.250	0.250	0.013	0.237	0.040	1.468
HD 193677	343.593132	−35.073332	8.396	7.760	7.600	0.160	0.008	0.152	0.025	2.196
HD 198592	353.432167	−39.866271	6.508	7.780	7.580	0.200	0.008	0.192	0.025	1.623
HD 198736	329.508381	−37.301504	5.965	8.630	8.340	0.290	0.008	0.282	0.025	2.193
HD 198752	6.960965	−39.376813	3.287	8.620	7.140	1.480	0.018	1.462	0.059	−0.335
HD 200203	337.197874	−39.987120	5.505	7.530	7.350	0.180	0.009	0.171	0.028	1.026
HD 200475	319.771576	−35.486409	4.474	8.080	7.820	0.260	0.021	0.239	0.065	1.008
HD 200670	7.258495	−41.851515	12.481	8.340	7.810	0.530	0.004	0.526	0.013	3.279
HD 201247	342.588946	−41.727507	28.760	7.700	7.100	0.600	0.004	0.596	0.013	4.381
HD 201292	310.233667	−31.637037	4.720	8.510	8.190	0.320	0.094	0.226	0.290	1.270
HD 201427	345.509006	−42.280150	20.650	7.730	7.068	0.662	0.005	0.657	0.016	3.627
HD 203244	324.896406	−38.909688	48.062	7.700	6.970	0.730	0.001	0.729	0.003	5.376
HD 204352	339.381016	−43.994561	5.251	8.660	8.400	0.260	0.008	0.252	0.025	1.977
HD 204370	347.479373	−45.467633	4.886	7.820	7.520	0.300	0.009	0.291	0.028	0.937
HD 205834	307.420813	−30.917878	4.261	9.340	8.110	1.230	0.093	1.137	0.301	0.956
HD 205877	344.098347	−46.530732	5.135	6.784	6.202	0.582	0.008	0.574	0.025	−0.271
HD 208094	305.516566	−29.818144	4.135	8.440	8.210	0.230	0.081	0.149	0.249	1.043

Table 10
(Continued)

Name …	l (deg)	b (deg)	ϖ (mas)	B (mag)	V (mag)	$(B-V)$ (mag)	$E(B-V)$ (mag)	$(B-V)_0$ (mag)	A_V (mag)	M_V (mag)
HD 208614	352.610492	−51.199348	3.686	7.870	7.720	0.150	0.009	0.141	0.028	0.525
HD 209234	331.450421	−46.325930	23.352	8.480	7.870	0.610	0.003	0.607	0.009	4.702
HD 209295	326.230432	−44.109185	8.528	7.570	7.320	0.250	0.005	0.245	0.015	1.959
HD 210572	338.681592	−50.347903	13.575	8.238	7.714	0.524	0.004	0.520	0.013	3.365
HD 212661	332.056482	−50.187132	6.910	7.080	6.910	0.170	0.005	0.165	0.015	1.092
HD 213669	336.103568	−53.075908	8.779	7.620	7.420	0.200	0.004	0.196	0.012	2.125
HD 214291	359.582222	−59.601060	10.317	7.120	6.590	0.530	0.003	0.527	0.009	1.648
HD 215573	309.029149	−35.525946	6.326	5.180	5.311	−0.131	0.009	−0.140	0.027	−0.711
HD 216668	317.189250	−45.028130	3.871	7.980	7.880	0.100	0.015	0.085	0.046	0.773
HD 216743	352.070787	−61.942147	9.768	7.413	7.247	0.166	0.003	0.163	0.009	2.187
HD 217522	346.722689	−61.851320	9.715	7.990	7.520	0.470	0.003	0.467	0.009	2.448
HD 218090	325.729448	−53.525332	5.474	8.420	8.130	0.290	0.006	0.284	0.019	1.803
HD 219301	326.385409	−55.844349	10.907	6.840	6.560	0.280	0.003	0.277	0.009	1.739
HD 220633	345.169775	−66.525355	2.200	8.770	8.290	0.480	0.009	0.471	0.028	−0.026
HD 222060	308.224592	−39.498589	6.123	6.900	5.983	0.917	0.009	0.908	0.029	−0.111
HD 223065	341.382354	−70.363573	12.000	7.400	7.120	0.280	0.002	0.278	0.006	2.510

ORCID iDs

Samuel N. Mellon https://orcid.org/0000-0003-3405-2864
Eric E. Mamajek https://orcid.org/0000-0003-2008-1488
Remko Stuik https://orcid.org/0000-0001-7797-3749
Konstanze Zwintz https://orcid.org/0000-0001-9229-8315
Matthew A. Kenworthy https://orcid.org/0000-0002-7064-8270
Geert Jan J. Talens https://orcid.org/0000-0003-4787-2335
Olivier Burggraaff https://orcid.org/0000-0002-2487-4533
John I. Bailey, III https://orcid.org/0000-0002-4272-263X
Patrick Dorval https://orcid.org/0000-0003-3812-2436
Blaine B. D. Lomberg https://orcid.org/0000-0002-1520-7851
Rudi B. Kuhn https://orcid.org/0000-0002-4236-9020
Michael J. Ireland https://orcid.org/0000-0002-6194-043X

References

Blažko, S. 1907, AN, 175, 325
Boro Saikia, S., Marvin, C. J., Jeffers, S. V., et al. 2018, A&A, 616, A108
Borucki, W. J., Koch, D., Basri, G., et al. 2010, Sci, 327, 977
Bos, M. 1994, ExA, 5, 13
Boss, B. 1937, General Catalogue of 33342 Stars for the Epoch 1950, Vol. 1 and 5 (Washington, DC: Carnegie Instit. Washington)
Bowman, D. M., & Kurtz, D. W. 2018, MNRAS, 476, 3169
Breger, M., & Pamyatnykh, A. A. 1998, A&A, 332, 958
Bressan, A., Marigo, P., Girardi, L., et al. 2012, MNRAS, 427, 127
Brown, A. G. A., Vallenari, A., Prusti, T., et al. 2018, A&A, 616, A1
Burggraaff, O., Talens, G. J. J., Spronck, J., et al. 2018, A&A, 617, A32
Buscombe, W. 1969, MNRAS, 144, 31
Capitanio, L., Lallement, R., Vergely, J. L., Elyajouri, M., & Monreal-Ibero, A. 2017, A&A, 606, A65
Cargile, P. A., James, D. J., Pepper, J., et al. 2014, ApJ, 782, 29
Collins, K. A., Collins, K. I., Pepper, J., et al. 2018, AJ, 156, 234
Corbally, C. J. 1984, ApJS, 55, 657
Cousins, A. W. J., & Lagerweij, H. C. 1971, MNSSA, 30, 12
Cucchiaro, A., Macau-Hercot, D., Jaschek, M., & Jaschek, C. 1977, A&AS, 30, 71
da Silva, R., Maceroni, C., Gandolfi, D., Lehmann, H., & Hatzes, A. P. 2014, A&A, 565, A55
De Cat, P. 2007, CoAst, 150, 167
De Mey, K., Daems, K., & Sterken, C. 1998, A&A, 336, 527
Dorval, P., Talens, G. J. J., Otten, G. P. P. L., et al. 2019, arXiv:1904.02733
Gallet, F., & Bouvier, J. 2013, A&A, 556, A36
Garrison, R. F., Hiltner, W. A., & Schild, R. E. 1977, ApJS, 35, 111
Gray, R. O., Corbally, C. J., Garrison, R. F., et al. 2006, AJ, 132, 161
Gray, R. O., & Garrison, R. F. 1987, ApJS, 65, 581
Gray, R. O., & Garrison, R. F. 1989, ApJS, 70, 623
Gray, R. O., Riggs, Q. S., Koen, C., et al. 2017, AJ, 154, 31
Groenewegen, M. A. T. 2018, A&A, 619, A8
Hartman, J. D., Bakos, G. Á., Kovács, G., & Noyes, R. W. 2010, MNRAS, 408, 475
Hiltner, W. A., Garrison, R. F., & Schild, R. E. 1969, ApJ, 157, 313
Houk, N. 1978, Michigan Catalogue of Two-dimensional Spectral Types for the HD Stars, Vol. 2 (Ann Harbor, MI: Michigan Univ. Press)
Houk, N. 1982, Michigan Catalogue of Two-dimensional Spectral Types for the HD Stars, Vol. 3 (Ann Arbor, MI: Michigan Univ. Press)
Houk, N., & Cowley, A. P. 1975, University of Michigan Catalogue of Two-dimensional Spectral Types for the HD Stars, Vol. I
Houk, N., Swift, C. M., Murray, C. A., Penston, M. J., & Binney, J. J. 1997, ESA Spec. Publ., 402, 279
Howell, S. B., Sobeck, C., Haas, M., et al. 2014, PASP, 126, 398
Hube, D. P. 1970, MmRAS, 72, 233
Hunter, J. D. 2007, Matplotlib: A 2D Graphics Environment, http://www.scipy.org/
Jones, E., Oliphant, T., Peterson, P., et al. 2001, SciPy: Open Source Scientific Tools for Python, http://www.scipy.org/
Kalas, P., Jinfei Wang, J., Wang, L., et al. 2019, AAS Meeting, 233, 218.03
Keenan, P. C., & McNeil, R. C. 1989, ApJS, 71, 245
Kenworthy, M. A., & Mamajek, E. E. 2015, ApJ, 800, 126
Kharchenko, N. V. 2001, KFNT, 17, 409
Kharchenko, N. V., & Roeser, S. 2009, yCat, 1280
Koen, C., & Eyer, L. 2002, MNRAS, 331, 45
Kurtz, D. W. 1980, MNRAS, 193, 61
Lallement, R., Capitanio, L., Ruiz-Dern, L., et al. 2018, A&A, 616, A132
Lefèvre, L., Marchenko, S. V., Moffat, A. F. J., & Acker, A. 2009, A&A, 507, 1141
Levato, H. 1975, A&AS, 19, 91
Levato, H., Malaroda, S., Morrell, N., Solivella, G., & Grosso, M. 1996, A&AS, 118, 231
Levenhagen, R. S., & Leister, N. V. 2006, MNRAS, 371, 252
Liakos, A., & Niarchos, P. 2017, MNRAS, 465, 1181
Luckas, P. 2018, ATel, 11460, 1
Mamajek, E. E., & Hillenbrand, L. A. 2008, ApJ, 687, 1264
Mamajek, E. E., Quillen, A. C., Pecaut, M. J., et al. 2012, AJ, 143, 72
Marigo, P., Girardi, L., Bressan, A., et al. 2017, ApJ, 835, 77
Mason, B. D., Wycoff, G. L., Hartkopf, W. I., Douglass, G. G., & Worley, C. E. 2019, yCat, 102026
Mékarnia, D., Chapellier, E., Guillot, T., et al. 2017, A&A, 608, 6
Mellon, S. N., Mamajek, E. E., Oberst, T. E., & Pecaut, M. J. 2017, ApJ, 844, 66
Mellon, S. N., Mamajek, E. E., Zwintz, K., et al. 2019a, ApJ, 870, 36
Mellon, S. N., Stuik, R., Kenworthy, M., et al. 2019b, AAS Meeting Abstracts, 233, 140.22

Mentel, R. T., Kenworthy, M. A., Cameron, D. A., et al. 2018, A&A, 619, A157
Miglio, A., Montalbán, J., & Dupret, M.-A. 2007, CoAst, 151, 48
Moe, M., & Kratter, K. M. 2018, ApJ, 854, 44
Montgomery, M. H., & Odonoghue, D. 1999, DSSN, 13, 28
Nagy, T. A. 1985, BAAS, 17, 887
Oberst, T. E., Rodriguez, J. E., Colón, K. D., et al. 2017, AJ, 153, 97
Ochsenbein, F., Bauer, P., & Marcout, J. 2000, A&AS, 143, 23
O'Connell, D. J. K. 1951, PRCO, 2, 85
Osborn, J., Föhring, D., Dhillon, V. S., & Wilson, R. W. 2015, MNRAS, 452, 1707
Paunzen, E., & Duffee, B. 1996, IBVS, 4297, 1
Paunzen, E., Duffee, B., Heiter, U., Kuschnig, R., & Weiss, W. W. 2001, A&A, 373, 625
Paunzen, E., Weiss, W. W., Kuschnig, R., et al. 1998, A&A, 335, 533
Pepper, J., Pogge, R. W., DePoy, D. L., et al. 2007, PASP, 119, 923
Perryman, M. A. C. 1997, ESA Spec. Publ., 1200
Pojmanski, G. 2002, AcA, 52, 397
Press, W. H., Teukolsky, S. A., Vetterling, W. T., & Flannery, B. P. 1992, Numerical Recipes in FORTRAN. The Art of Scientific Computing (Cambridge: Cambridge Univ. Press)
Pribulla, T., Kreiner, J. M., & Tremko, J. 2003, CoSka, 33, 38
Pribulla, T., Vaňko, M., Chochol, D., Hambálek, L., & Parimucha, Š. 2011, AN, 332, 607
Rabus, M., & Prieto, J. L. 2018, ATel, 11506, 1
Rimoldini, L., Dubath, P., Süveges, M., et al. 2012, MNRAS, 427, 2917
Rodríguez, E., López-González, M. J., & López de Coca, P. 2000, A&AS, 144, 469
Rossum, G. 1995, Python Reference Manual, CWI Rep. CS-R9525, (Amsterdam: Centrum voor Wiskunde en Informatica)
Sahade, J. 1952, ApJ, 116, 35
Scargle, J. D. 1982, ApJ, 263, 835
Shappee, B. J., Prieto, J. L., Grupe, D., et al. 2014, ApJ, 788, 48
Shara, M. M., Moffat, A. F. J., Gerke, J., et al. 2009, AJ, 138, 402
Sitek, M., & Pojmański, G. 2014, AcA, 64, 115
Soderblom, D. R. 1990, AJ, 100, 204
Sota, A., Maíz Apellániz, J., Morrell, N. I., et al. 2014, ApJS, 211, 10
Stanek, K. Z., Holoien, T. W. S., Kochanek, C. S., et al. 2018, ATel, 11454, 1
Stéfan van der Walt, S. C. C., & Varoquaux, G. 2011, The NumPy Array: A Structure for Efficient Numerical Computation, http://www.scipy.org/
Sterken, C. 1997, A&A, 325, 563
Stobie, R. S., & Shobbrook, R. R. 1976, MNRAS, 174, 401
Strader, J., Chomiuk, L., Holoien, T. W. S., et al. 2018, ATel, 11456, 1
Stuik, R., Bailey, J. I., Dorval, P., et al. 2017, A&A, 607, A45
Talens, G. J. J., Albrecht, S., Spronck, J. F. P., et al. 2017a, A&A, 606, A73
Talens, G. J. J., Deul, E. R., Stuik, R., et al. 2018, A&A, 619, A154
Talens, G. J. J., Spronck, J. F. P., Lesage, A.-L., et al. 2017b, A&A, 601, A11
Terrell, D., Munari, U., Zwitter, T., & Nelson, R. H. 2003, AJ, 126, 2988
The Astropy Collaboration, Price-Whelan, A. M., Sipőcz, B. M., et al. 2018, AJ, 156, 123
Torres, C. A. O., Quast, G. R., da Silva, L., et al. 2006, A&A, 460, 695
Udalski, A., Szymanski, M. K., Soszynski, I., & Poleski, R. 2008, AcA, 58, 69
van Leeuwen, F. 2007, A&A, 474, 653
van Werkhoven, T. I. M., Kenworthy, M. A., & Mamajek, E. E. 2014, MNRAS, 441, 2845
Watson, C. L., Henden, A. A., & Price, A. 2006, SASS, 25, 47
Wenger, M., Ochsenbein, F., Egret, D., et al. 2000, A&AS, 143, 9
Wilsey, N. J., & Beaky, M. M. 2009, SASS, 28, 107
Young, A. T. 1967, AJ, 72, 747
Zwintz, K., Fossati, L., Ryabchikova, T., et al. 2014a, Sci, 345, 550
Zwintz, K., Reese, D. R., Neiner, C., et al. 2019, A&A, 627, A28
Zwintz, K., Ryabchikova, T., Lenz, P., et al. 2014b, A&A, 567, A4